Engineering Analysis with Boundary Elements 145 (2022) 363–395

Contents lists available at ScienceDirect

Engineering Analysis with Boundary Elements

journal homepage: www.elsevier.com/locate/enganabound

Optimization of MLP neural network for modeling flow boiling performance of Al_2O_3/water nanofluids in a horizontal tube

Mahyar Ghazvini [a], Seyyed Mojtaba Varedi-Koulaei [b], Mohammad Hossein Ahmadi [b], Myeongsub Kim [a,*]

[a] Department of Mechanical Engineering, Florida Atlantic University, 777 Glades Road, Boca Raton, FL 33431, United States
[b] Faculty of Mechanical and Mechatronics Engineering, Shahrood University of Technology, Shahrood, Iran

ARTICLE INFO

Keywords:
Flow boiling
MLP neural network
Swarm-based optimization algorithms
Nanofluid

ABSTRACT

In this paper, a multilayer perceptron (MLP) artificial neural network (ANN) with a back-propagation (BP) training algorithm is applied for modeling thermophysical properties and subcooled flow boiling performance of Al_2O_3/water nanofluid in a horizontal tube. The influence of nanofluid concentration, heat flux, and flow rate on different thermophysical parameters, including thermal conductivity, thermal conductivity enhancement, viscosity, viscosity enhancement, and heat transfer coefficient, are investigated. Specifically, flow boiling of Al_2O_3/water nanofluid in a horizontal tube is modeled with the MLP neural network optimized by three novel swarm-based optimization algorithms: namely, Equilibrium Optimizer (EO), Marine Predators Algorithm (MPA), and Slime Mould Algorithm (SMA). To evaluate the effectiveness of different models, the MSE (Mean-Square Error) of the ANN model with varying optimization algorithms is calculated and compared. Additionally, the optimal network and regression values for each parameter are determined. The results show that the applied neural network and optimization algorithms could model the thermal conductivity, thermal conductivity enhancement, and viscosity better than the viscosity enhancement and heat transfer coefficient. The MSE of the best network for the thermal conductivity is 2.693×10^{-7}, while the MSE of the best network for the viscosity enhancement is 0.0598. Also, the EO algorithm achieves the best optimization for the first three outputs, thermal conductivity, thermal conductivity enhancement, and viscosity. In comparison, the MPA algorithm extracts the optimal network for the other two outputs, viscosity enhancement, and heat transfer coefficient.

1. Introduction

The accelerated growth of nanotechnology and microelectronics placed significant issues in cooling systems of intense heat loads released from tightly bounded surfaces in many electrical devices. Conventional working fluids are often unsuccessful to cool down such devices leading to serious damage. On the other hand, nanofluids have demonstrated excellent cooling performance in many applications. They have enhanced the thermal performance of working fluid significantly compared with conventional fluid due to its exceptional heat transfer properties of dispersed solid particles [1,2]. Choi [3] pioneered using 1–100 nm nanoparticles dispersed in a base fluid to enhance thermophysical properties such as viscosity and thermal conductivity. After that, many scholars have investigated different nanofluids by adding metallic, non-metallic, or combination of other nanoparticles to have hybrid nanofluids, e.g., Cu nanoparticles in water [4], Al_2O_3 nanoparticles in water [5], AlN nanoparticles in water [6], CuO nanoparticle in R-113 refrigerant [7,8], Fe_3O_4 nanoparticle in water [9], CuO and SiO_2 nanoparticle-based R-134a refrigerant [10], TiO_2 nanoparticles in water [11], ZnO nanoparticles in water [12], carbon nanotube in therminol 66 [13] in different heat transfer applications such as in solar energy systems [14,15], domestic refrigerators [16], air conditioning systems [17], heat exchangers [18], heat pipes [16,17] and thermosiphons [19].

The presence of nanoparticles in a base fluid substantially improves the heat transfer capability due to the thermal conductivity enhancement [20]. At the same time, the fluid flow characteristics are also affected by rising the viscosity. Therefore, measurements of heat transfer and fluid properties have been considered important in nanofluid applications. In 2003, flow boiling experiment with nanofluid was initially performed by Faulkner et al. [21]. Both improvement and degradation of Al_2O_3/H_2O nanofluid flow boiling were found in their experiment. In another experiment, Cu/R114 nanofluid flow boiling was investigated

* Corresponding author.
E-mail address: kimm@fau.edu (M. Kim).

https://doi.org/10.1016/j.enganabound.2022.09.034
Received 4 May 2022; Received in revised form 27 September 2022; Accepted 28 September 2022
Available online 7 October 2022

Nomenclature

y_d	desired output
y_g	generated output
fit	fitness value
l	current iteration
L	maximum number of iteration
ub	upper bound
lb	lower bound
N	number of neuron
F	transfer function
X	optimization variables

Greek Letters

α	leader
β	subordinates
δ	subordinates
ω	subordinates

Subscripts

i	*i*th
j	*j*th

Abbreviation

HL	hidden layer
EO	equilibrium optimizer
MSE	mean-square error
BP	back-propagation
LSSVM	least-squares support-vector machine
RBF	radial basis function
GNN	genetic neural network
ANN	artificial neural network
MLP	multilayer perceptron
MPA	marine predators algorithm
SMA	slime mould algorithm
PSO	particle swarm optimization

by Peng et al. [8]. Their outcomes show that the flow boiling heat transfer is escalated by about 29.7 percent when the mass fraction of nanoparticles is 0.5 wt%. Since then, several works on the nanofluid flow boiling have been published, and the thermophysical properties of nanofluid have also been under consideration [22–27]. For instance, Wang et al. [28] experimentally studied the effects of Graphite/H_2O and SiC/H_2O nanofluids on flow boiling heat transfer, and both the improvement and degradation have been reported. The enhancement's reason is the improvement of the thermophysical properties because of the random motion of nanoparticles.

On the other hand, the deterioration is induced by the decrease in the number of nucleation sites because of the deposition of nanoparticles. Additionally, it was reported which the Brownian motion of nanoparticles alters the boundary layer's structure, and therefore, the flow boiling heat transfer is improved [8]. Most investigations have focused on viscosity and thermal conductivity of nanofluids in flow boiling heat transfer because the use of nanofluids in engineering applications have both drawbacks and advantages. Hence, the effect of nanofluids on flow boiling heat transfer and critical thermophysical properties including viscosity and thermal conductivity should be taken into consideration.

Many studies have employed nanofluid in flow boiling heat transfer under a subcooled region for cooling microelectronic devices. Subcooled flow boiling appears once the bulk liquid temperature remains below the saturation temperature at a given pressure. This regime is characterized by dominant convection and phase change phenomena that provide high heat transfer rates at small wall superheat. This is why subcooled flow boiling has been widely used for cooling technologies in different engineering applications, especially microelectronic devices. For example, Zangeneh et al. Field [28] theoretically and experimentally studied forced convection and subcooled flow boiling of CuO-water nanofluid to understand the influences of different parameters, including subcooling temperature, heat flux, nanofluid concentration, and fluid flow rate on the thermal performance of a vertical tube. Their results show that the heat transfer coefficient decreases by augmenting the subcooling temperature, while the behavior is the opposite for the fluid flow rate and heat flux. Also, heat transfer coefficients of subcooled flow boiling for gamma-alumina/water nanofluid was experimentally investigated by Karimzadehkhouei et al. [29]. Based on their results, heat transfer coefficients of subcooled flow boiling for nanofluids with low mass fractions and pure water were approximately identical. Nonetheless, heat transfer performance was worsened for nanofluids with high mass fractions because of the additional thermal resistance and nucleation site decrease because of the nanofluid deposition [25, 30].

The disagreement on the enhancement or deterioration of nanofluid in flow boiling heat transfer has lasted long. Also, conducting two-phase flow boiling experiments or full CFD simulations require a high cost and time commitment. Heat transfer and thermophysical parameters like thermal conductivity, thermal conductivity enhancement, viscosity, viscosity enhancement, and heat transfer coefficient in boiling are usually a function of many independent variables including liquid and wall temperatures, each of them valid over a finite range of values. The relationship between these parameters and their relevance can be deduced using new computing techniques. A promising technique which can be applied is the use of soft-computing. In the past three decades, unprecedented development of soft computing techniques have been seen, such as Artificial Neural Networks (ANNs), Genetic Algorithm (GA), Genetic Programming (GP), Fuzzy-logic Control, and Data Mining, and its application to many scientific and engineering practices. Out of these, ANNs, which are inspired by biological nervous systems of humans, learn to perform tasks by utilizing available data, without the need for programmed task-specific rules. Artificial neural network (ANN) can achieve a universal correlation and acceptable prediction accuracy for all experimental data [31]. The artificial neural network (ANN) has been effectively implemented in numerous engineering and scientific practices, including data mining, pattern recognition, and system identification. However, limited studies have been performed to model flow boiling heat transfer using the ANN. In this paper, a multilayer perceptron (MLP) ANN with a back-propagation (BP) training algorithm is applied for modeling thermophysical properties and subcooled flow boiling performance of Al_2O_3/water nanofluid in a horizontal tube. The MLP neural network was optimized by three novel swarm-based optimization algorithms, namely: Equilibrium Optimizer (EO), Marine Predators Algorithm (MPA), and Slime Mould Algorithm (SMA), to model flow boiling of Al_2O_3/water nanofluid. To the best of the authors' knowledge, it is the first time that MLP neural network has been optimized by three novel swarm-based optimization algorithms to accurately model flow boiling heat transfer. All steps of the neural network's design and the optimization process were implemented using MATLAB software.

2. Data gathering

All data used in this study for modeling five different thermophysical properties are obtained from previous experimental studies related to forced subcooled flow boiling heat transfer with Al_2O_3/water nanofluid in a horizontal tube [32–34]. The data show that nanofluid enhances the heat transfer coefficient by as much as 26% in the flow boiling

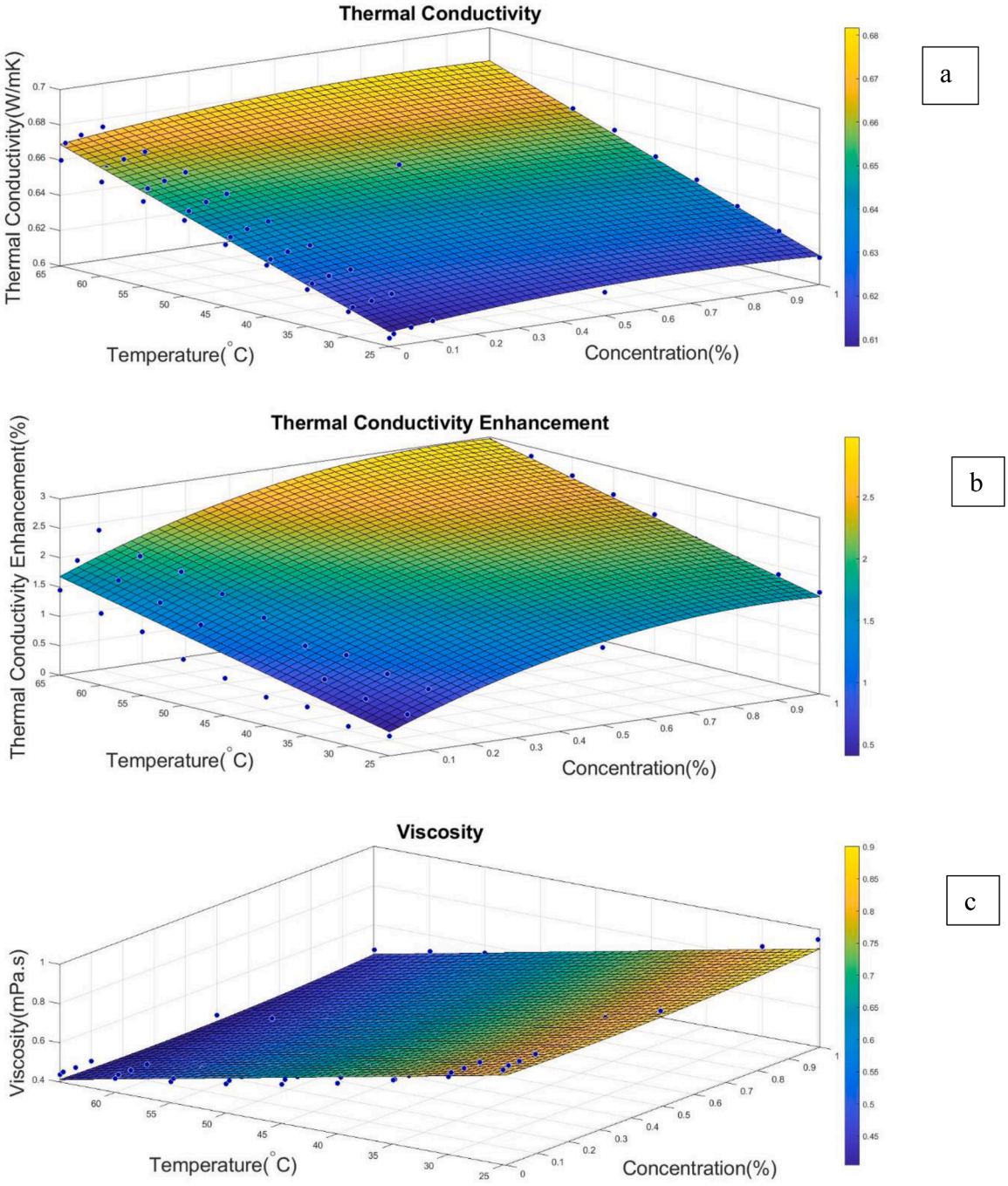

Fig. 1. 3D plots of (a) thermal conductivity, (b) thermal conductivity enhancement, (c) viscosity, (d) viscosity enhancement, and (e) heat transfer coefficient [32–34].

experimentation compared with conventional working fluids. This study evaluates the influences of nanofluid concentration, temperature, heat flux, and flow rate on thermophysical parameters of flow boiling. These parameters are thermal conductivity, thermal conductivity enhancement, viscosity, viscosity enhancement, and heat transfer coefficient. 3-D plots of all five parameters concerning different nanofluid concentrations, temperatures, heat fluxes, and flow rates are depicted in Fig. 1 [32–34].

3. Neural network structure

An artificial neural network (ANN) is an information processing machine invented for modeling the operation of a biological neural network of the brain. Neurons (the processing units of the network) are connected using communication links, each with an associated weight (the strength of the connection between units). An standard neural network builds from many neurons and connections [35]. The three principal elements of an ANN are a network architecture, a learning algorithm, and a transfer function. Each ANN method is different from the rest, according to these elements. The current study employs a multilayer perceptron (MLP)-type ANN model architecture with a back-propagation (BP) training algorithm. In the BP training algorithm, on the basis of the supervised learning strategy, the weights of the neuron's connections are modified in accordance with the difference

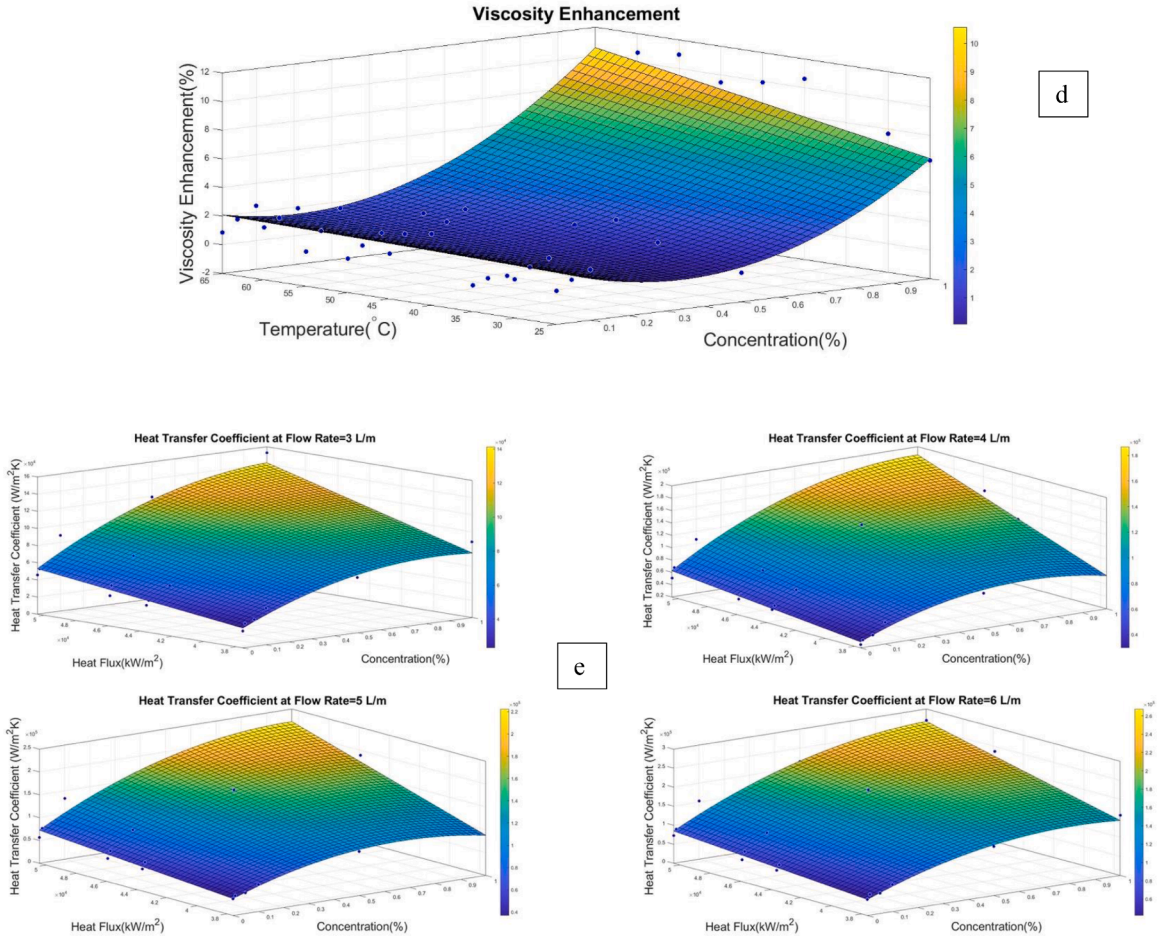

Fig. 1. (*continued*).

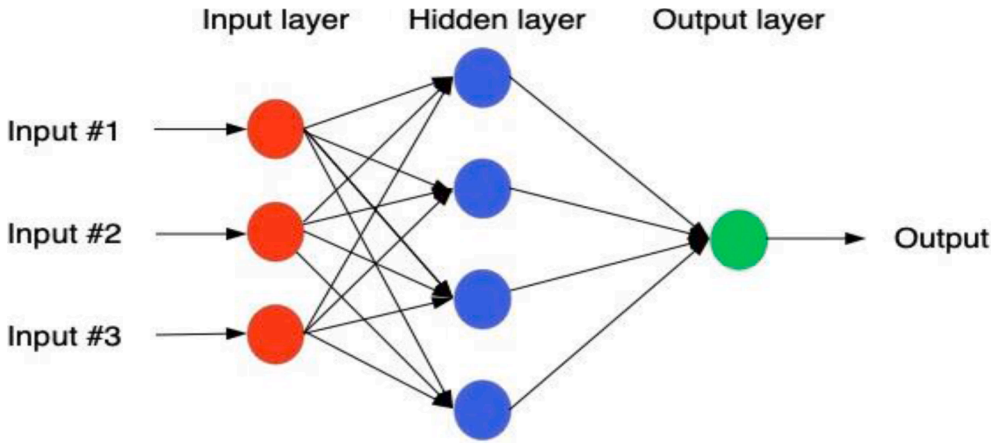

Fig. 2. Schematic of a neural network structure.

between the desired and the predicted network outputs [36].

The MLP network includes an input layer, one or more hidden layers, and an output layer (Fig. 2). The neurons' number in the input and output layers relies upon the number of input and output parameters of the problem. In contrast, the number of hidden layers and the number of neurons in each hidden layer can be chosen by the designer. Also, the transfer function of the neurons in the hidden and output layers can be selected by the designer. These selectable parameters determine the performance of the MLP network. To create a network with the best performance and lowest error, the architecture of the network has been optimized. The architecture parameters of this optimization problem consist of the neurons' number in each hidden layer and the transfer function of each layer.

This study considers the number of hidden layers as one, two, three, and four. Therefore, the optimization problem for the one hidden layer (1HL), two hidden layers (2HL), three hidden layers (3HL), and four hidden layers (4HL) networks has two, four, six, and eight design variables, respectively, as presented in Eqs. (1)–(4),

$$X_{1HL} = [N_1, F_1]^T \tag{1}$$

Table 1
Input variables and the number of samples for each output in a neural network.

Output	Inputs	N_S
Thermal conductivity (W/mK)	• Concentration (%)-wt. Al_2O_3/water • Temperature (°C)	54
Thermal conductivity enhancement (%)	• Concentration (%)-wt. Al_2O_3/water • Temperature (°C)	45
Viscosity (mPa.s)	• Concentration (%)-wt. Al_2O_3/water • Temperature (°C)	45
Viscosity enhancement (%)	• Concentration (%)-wt. Al_2O_3/water • Temperature (°C)	45
Heat transfer coefficient (W/m^2K)	• Concentration ((%)- wt.) • Heat flux (kW/m^2) • Flow rate (L/m)	96

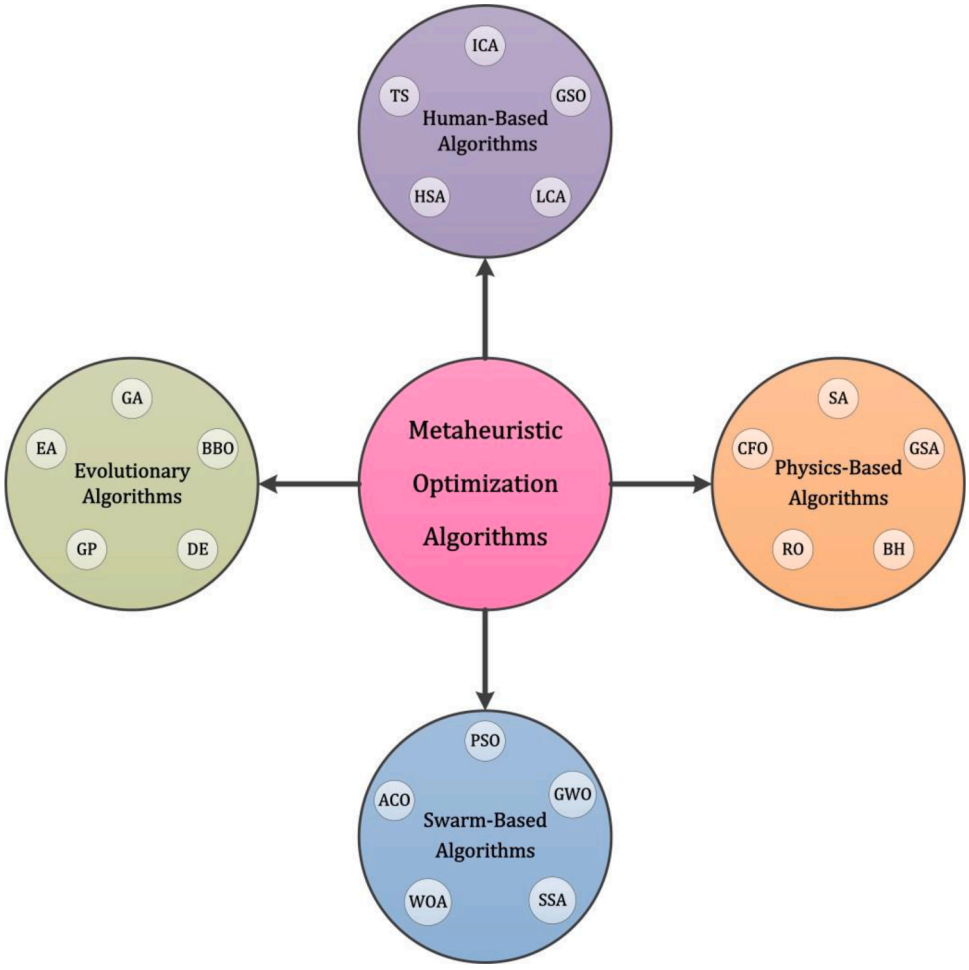

Fig. 3. Classification of metaheuristic algorithms.

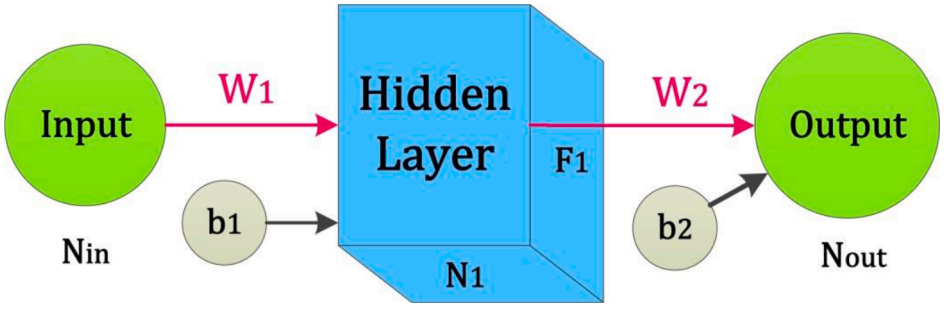

Fig. 4. Typical structure of the 1HL neural network.

Table 2
The best results for the 1HL network.

	N_1	F_1	MSE	R
Thermal Conductivity (Case 1)	4	tansig	8.1188e-07	0.99904
Thermal Conductivity Enhancement (Case 2)	26	logsig	0.001	0.99893
Viscosity (Case 3)	5	elliotsig	2.4214e-05	0.99945
Viscosity Enhancement (Case 4)	16	tansig	0.5423	0.97371
Heat Transfer Coefficient (Case 5)	9	tansig	33.7358	0.99532

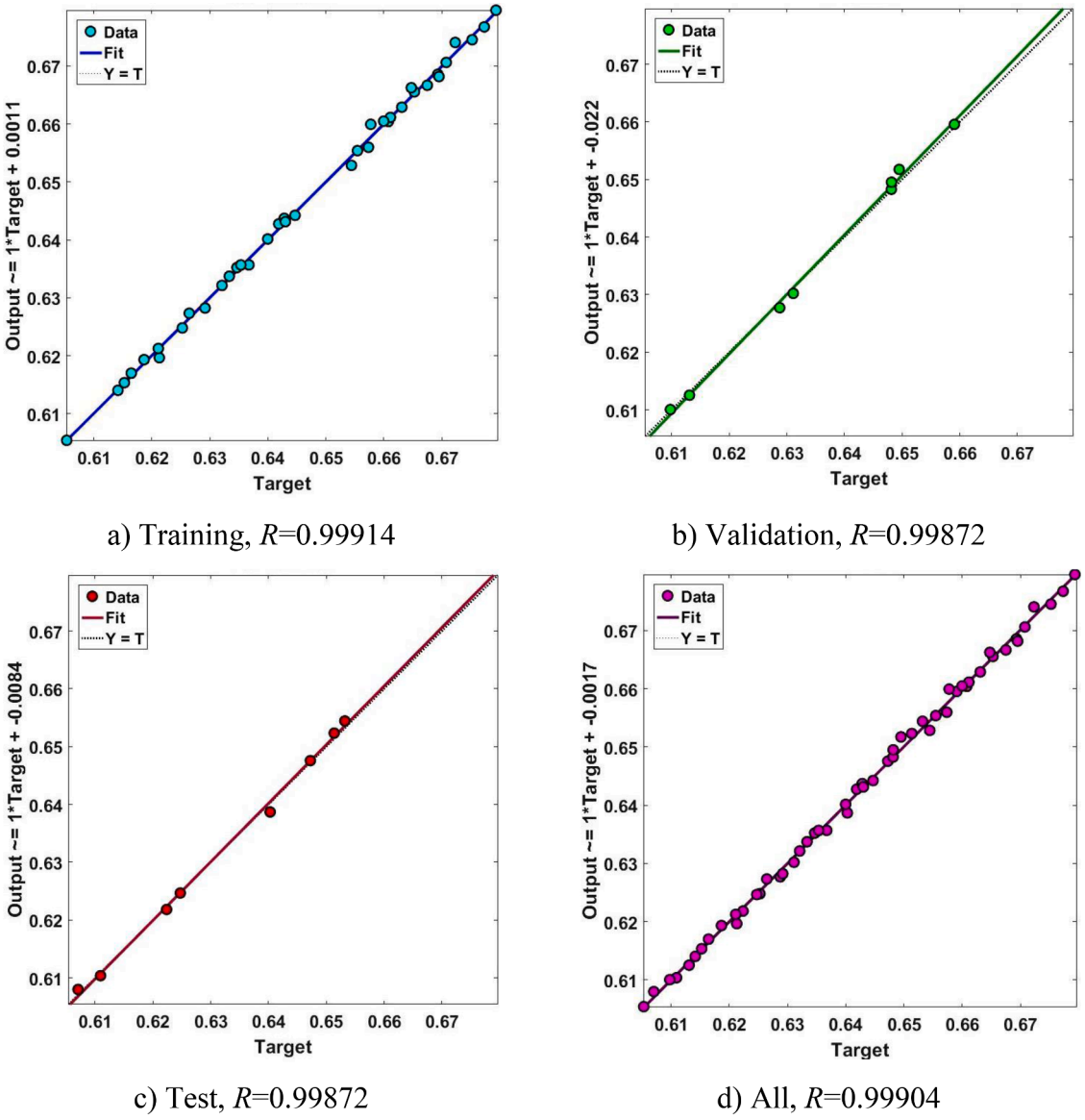

Fig. 5. Regression diagrams of the best MLP network for Case 1 with 1HL network.

$$X_{2HL} = [N_1, N_2, F_1, F_2]^T \tag{2}$$

$$X_{3HL} = [N_1, N_2, N_3, F_1, F_2 F_3]^T \tag{3}$$

$$X_{4HL} = [N_1, N_2, N_3, N_4, F_1, F_2 F_3, F_4]^T \tag{4}$$

X is the optimization variables for two, three, and four hidden-layer networks. N_i,F_i,and$T$are the number of neurons, the type of the transfer function, and the transpose of the design variable matrix in the ith hidden layer, respectively. The optimization of the ANN's performance is determined by the value of the mean squared error (MSE).

$$MSE = \frac{1}{N_S}\sum \left(y_d - y_g\right)^2 \tag{5}$$

where N_S is the number of samples, and y_d and y_g are the desired and generated outputs, respectively. Eq. (6) presents a summary of the optimization problem,

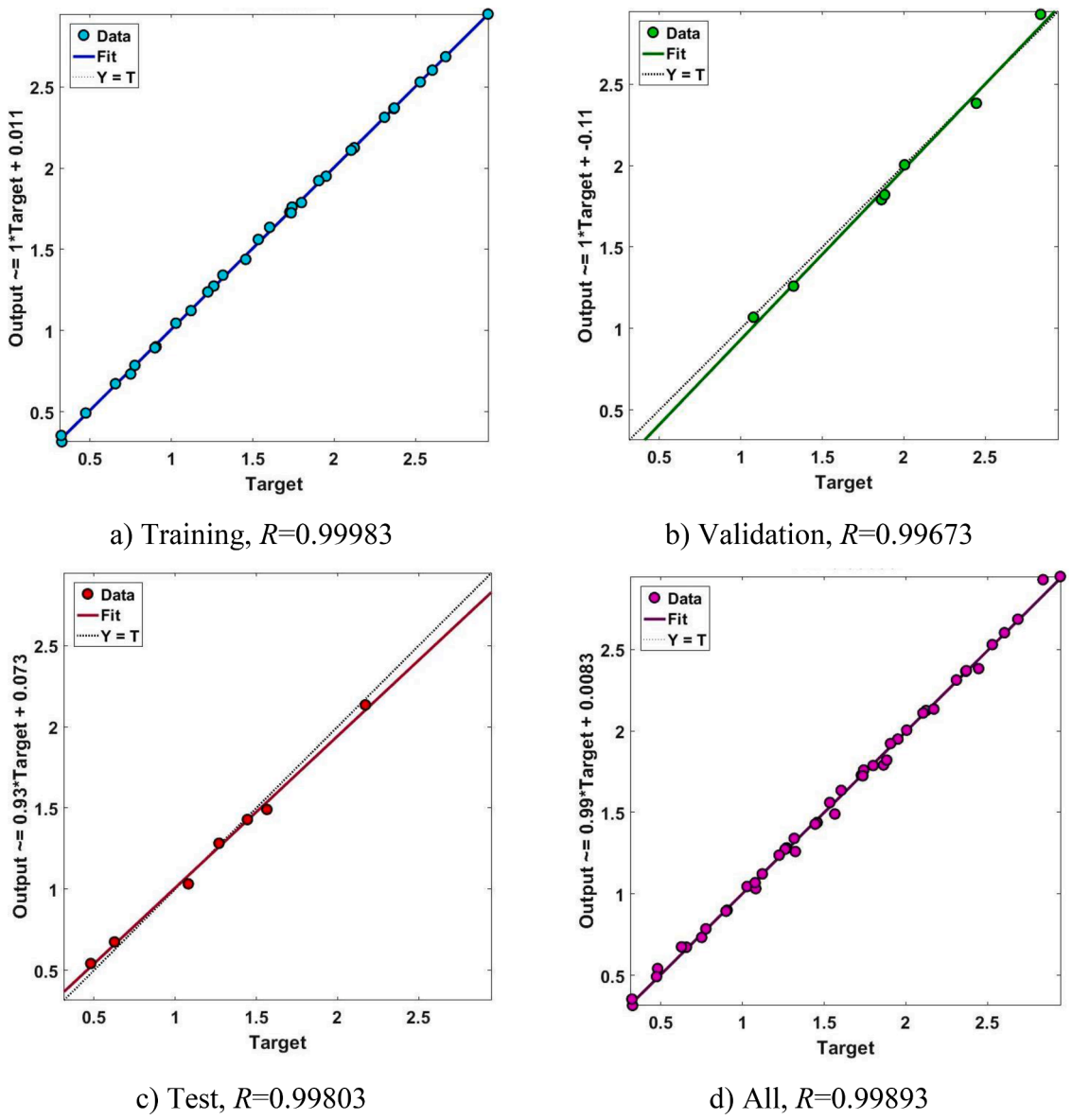

Fig. 6. Regression diagrams of the best MLP network for Case 2 with 1HL network.

$$\begin{gathered} MinMSE(X) \\ X:\{N_i,F_i\} \\ S.t(subject\ to): \\ F_i \in \{logsig, tansig, elliotsig\} \\ i=1,2 For\ 2HL\ network \\ i=1,2,3 For\ 3HL network \\ i=1,2,3,4 For\ 4HL network \end{gathered} \tag{6}$$

In Eq. (6), it is assumed that the transfer function is selected from the most commonly used transfer functions in ANN; Log-sigmoid transfer function (sigmoid), Hyperbolic tangent sigmoid transfer function (tansig), and Elliot symmetric sigmoid transfer function (elliotsig), as expressed in Eqs. (7)–(9).

$$F_{logsig}(x)=\frac{1}{1+e^{-x}}=\frac{e^{x}}{e^{x}+1} \tag{7}$$

$$F_{tansig}(x)=\tanh(x)=\frac{e^{x}-e^{-x}}{e^{x}+e^{-x}} \tag{8}$$

$$F_{elliotsig}(x)=\frac{x}{1+|x|} \tag{9}$$

The upper and lower bounds for the neurons' number in each hidden layer are 1 and 30, respectively, a commonly considered range in ANN-based modeling. The design parameters of this optimization are discrete variables, and the optimization algorithms must search for optimal variables to be integer values. The dataset is divided randomly that the first 70% of the collected samples are used for training, the other 15% for validation, and the last 15% for testing. The training dataset is used to train the model, and test dataset is used to test the trained model.

It is exclusively a designer's choice to partition datasets into training, testing, and validation. In general, most of the datasets are selected for training (typically more than 50%), and the remaining is split into two other sets. It is possible to select other values, not 70, but the common values for this separation are known to be 70%-15%-15%, as used in several papers [37–43]. Moreover, for training the network, the Levenberg-Marquardt algorithm was used. The validation error is checked automatically to prevent "overfitting". If the validation error is increased during 6 epochs in a row, the simulation is terminated.

The coefficient of determination, R, is another important criterion in measuring the quality of a neural network. It can be calculated as follows:

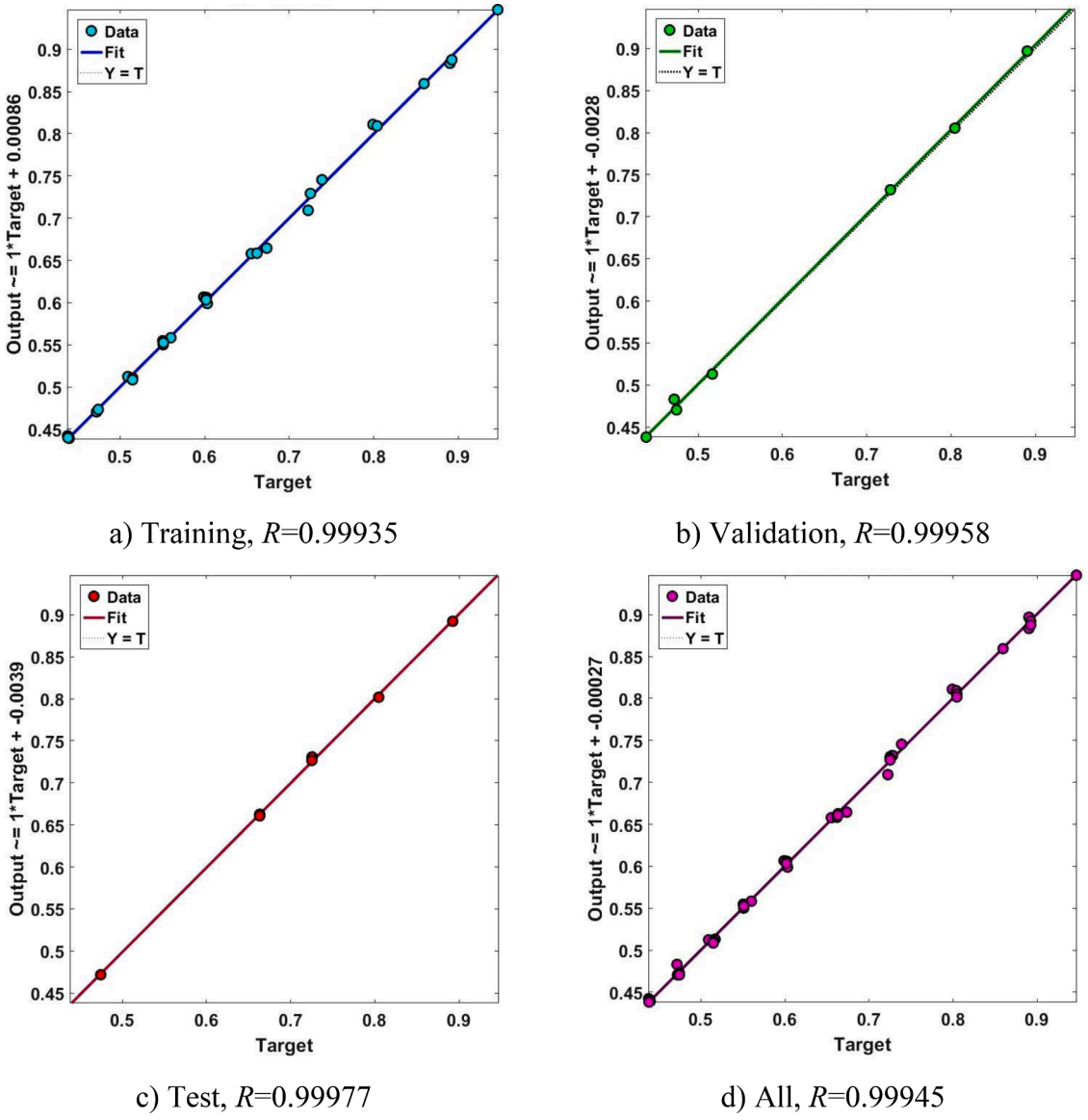

Fig. 7. Regression diagrams of the best MLP network for Case 3 with 1HL network.

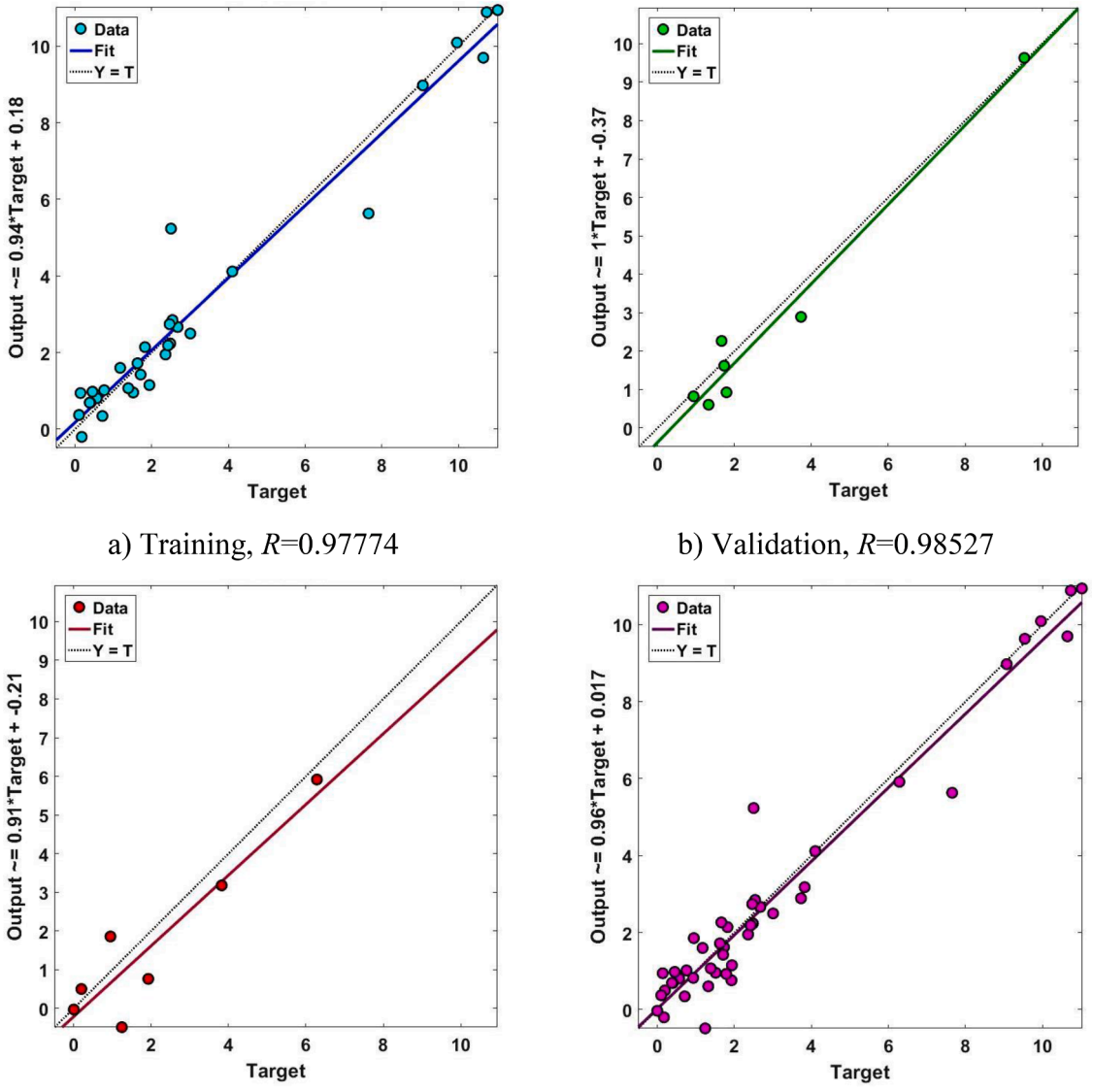

Fig. 8. Regression diagrams of the best MLP network for Case 4 with 1HL network.

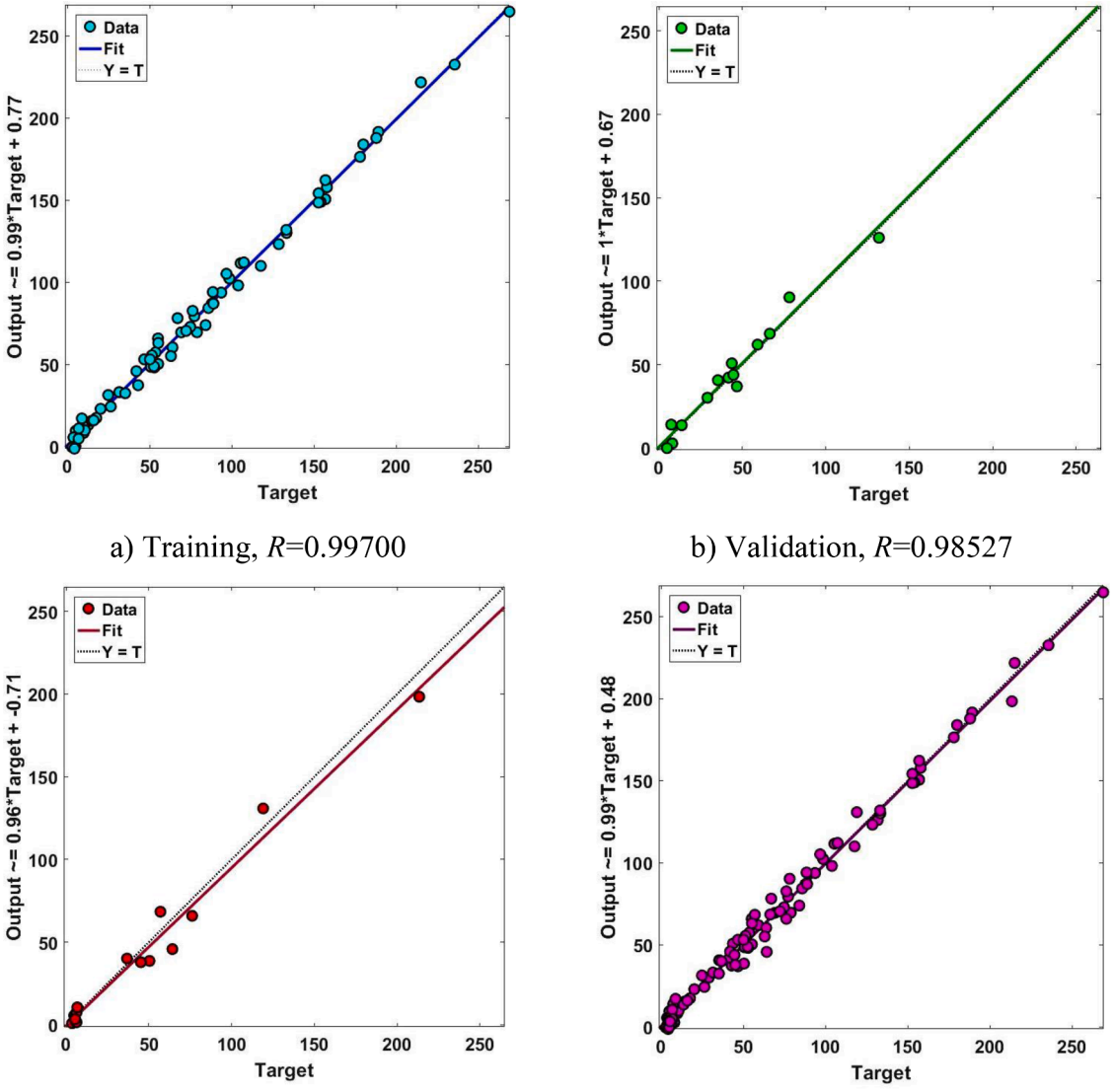

Fig. 9. Regression diagrams of the best MLP network for Case 5 with 1HL network.

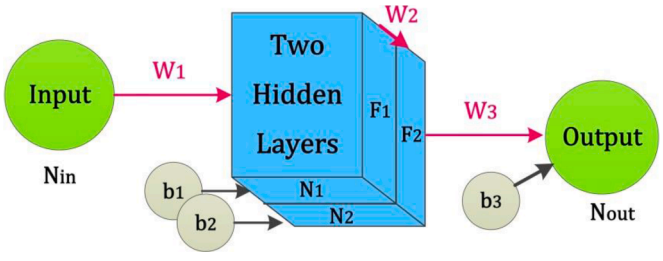

Fig. 10. A structure of the 2HL network.

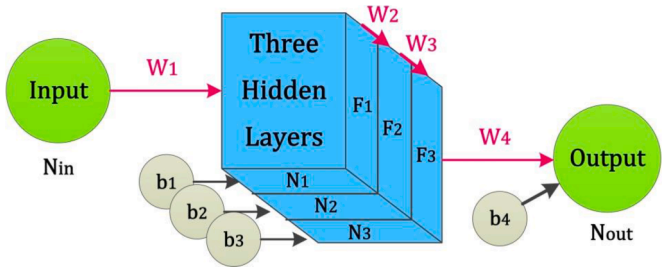

Fig. 11. A structure of the 3HL network.

$$R = \sqrt{1 - \frac{\sum_{i=1}^{N_s}(y_d - y_g)^2}{\sum_{i=1}^{N_s}(y_d - \bar{y}_d)^2}} \tag{10}$$

Where $\bar{y}_d$ is the mean of the actual outputs. It can be concluded from Eq. (10) that the maximum value of R is equal to 1. This condition ($R=1$) shows that the network predicts all the outputs accurately, without any error. Thus, when the value of R is closer to 1, the network's quality is higher.

The optimization algorithms are used to model the following five flow and heat transfer parameters in subcooled flow boiling with Al_2O_3/water nanofluid;

- Thermal conductivity
- Thermal conductivity enhancement
- Viscosity
- Viscosity enhancement

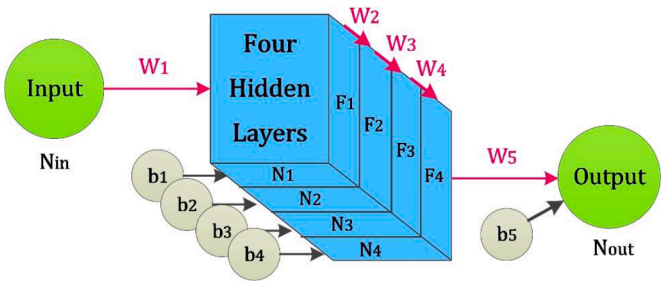

Fig. 12. A structure of the 4HL network.

Table 3
Optimum values of the design parameters for Case 1.

Network	Algorithms	N_i (number of neurons)	F_i (transfer function)	MSE	R
2HL	EO	[4 2]	[logsig tansig]	2.6935e-07	0.99968
	MPA	[6 6]	[tansig tansig]	3.6017e-07	0.99958
	SMA	[6 1]	[tansig tansig]	8.1578e-07	0.99903
3HL	EO	[4 2 2]	[logsig logsig logsig]	3.4525e-07	0.99959
	MPA	[5 3 6]	[logsig logsig tansig]	4.2032e-07	0.99950
	SMA	[4 4 4]	[tansig tansig tansig]	1.1345e-06	0.99867
4HL	EO	[4 14 9 4]	[elliotsig tansig elliotsig tansig]	8.9463e-07	0.99896
	MPA	[5 16 22 9]	[tansig tansig tansig logsig]	1.2406e-06	0.99862
	SMA	[4 1 1 1]	[tansig logsig tansig tansig]	8.7855e-07	0.99895

- Heat transfer coefficient

The input variables and the number of samples for each case are shown in Table 1.

4. Optimization algorithms

Three different metaheuristic optimization algorithms are applied to reduce the modeling errors. The metaheuristic algorithms solve optimization problems by imitating them to biological, physical, or social phenomena. They could be classified into four main categories: evolution, physics, swarm, and human-based methods, as shown in Fig. 3 [44]. Evolution-based methods are derived from the natural evolution laws. The strength of these methods is that the next generation of individuals is formed by combining the best current individuals. This enables the optimization of the population can be performed over the course of generations. The best known evolution-inspired method is the Genetic Algorithms (GA) [45] which imitate the Darwinian evolution. Physics-based methods mimics the physical rules in the universe. The best known algorithm in this group is the Simulated Annealing (SA), which Pincus developed in 1970 [46]. The third group consists of swarm-based methods that imitate the social behavior of animal groups. The best known algorithm in this group is the Particle Swarm Optimization (PSO), developed by Kennedy and Eberhart in 1995 [47]. It is inspired by the social behavior of bird flocking. There are also other metaheuristic methods inspired by human behaviors in the last group.

In the current study, three recently developed metaheuristic algorithms, namely, Equilibrium Optimizer (EO), Marine Predators Algorithm (MPA), and Slime Mould Algorithm (SMA), appeared in 2020, are considered. EO falls into the physics-based algorithms, while MPA and SMA are categorized as swarm-based algorithms. This study applies these algorithms because they are novel high-performance optimizers that can outperform well-known algorithms such as GA and PSO [48–50]. By varying the design variables, we aim to minimize the MSE value of the MLP neural network.

4.1. Equilibrium optimizer (EO)

The Equilibrium Optimizer (EO) is a physics-based algorithm whose inspiration is a simple well-mixed dynamic mass balance on a control volume. The mass balance equation gives the fundamental physics for the conservation of mass entering, leaving, and generated in a control volume. A first-order ordinary differential equation stating the generic mass-balance equation [51], in which the mass change in time is equivalent to the sum of the amount of mass that enters the system plus the amount being generated inside and the amount that leaves the system. In EO, each particle in a control volume (solution) with its

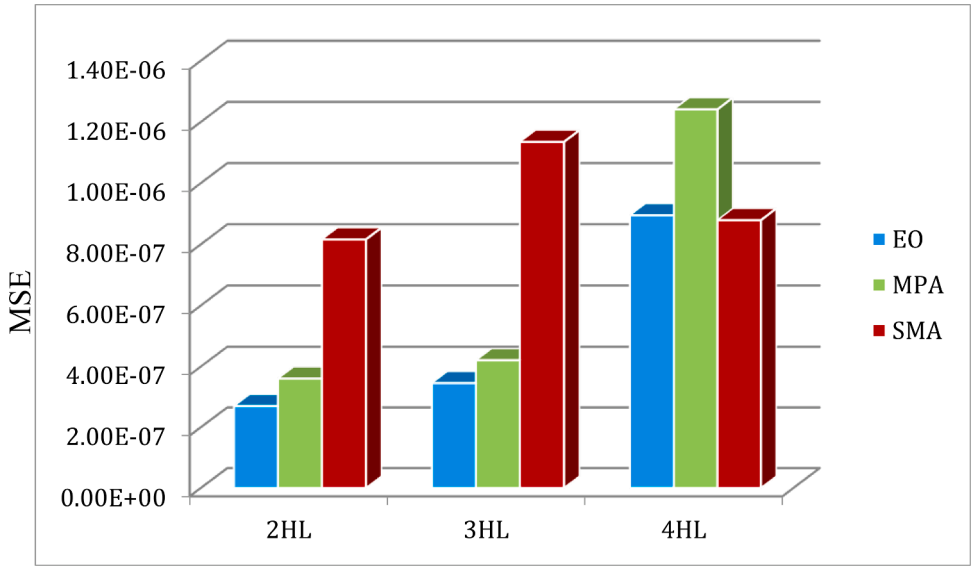

Fig. 13. Comparison between MSE errors for Case 1 with 2HL, 3HL and 4HL networks.

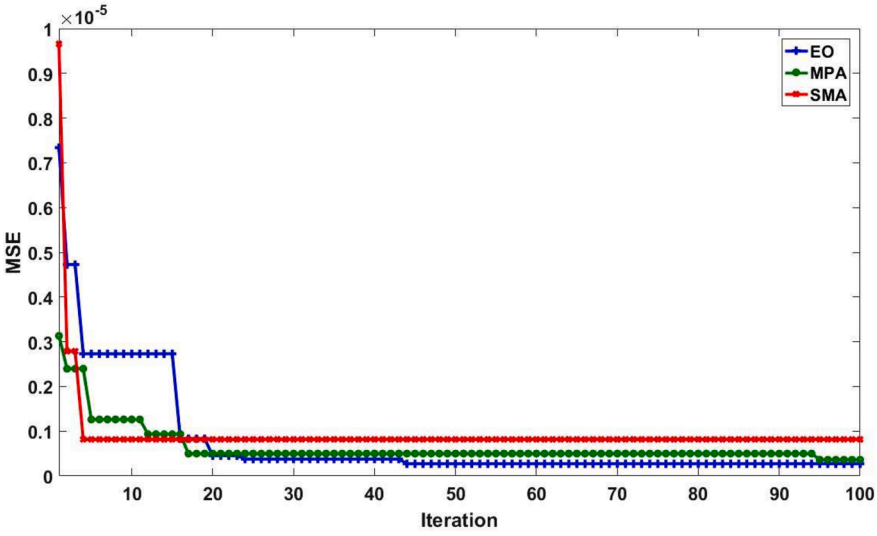

a) 2HL network

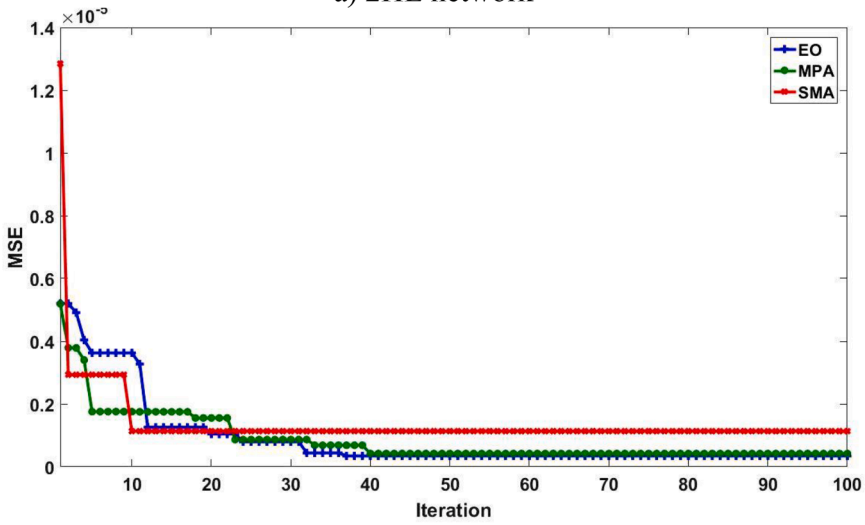

b) 3HL network

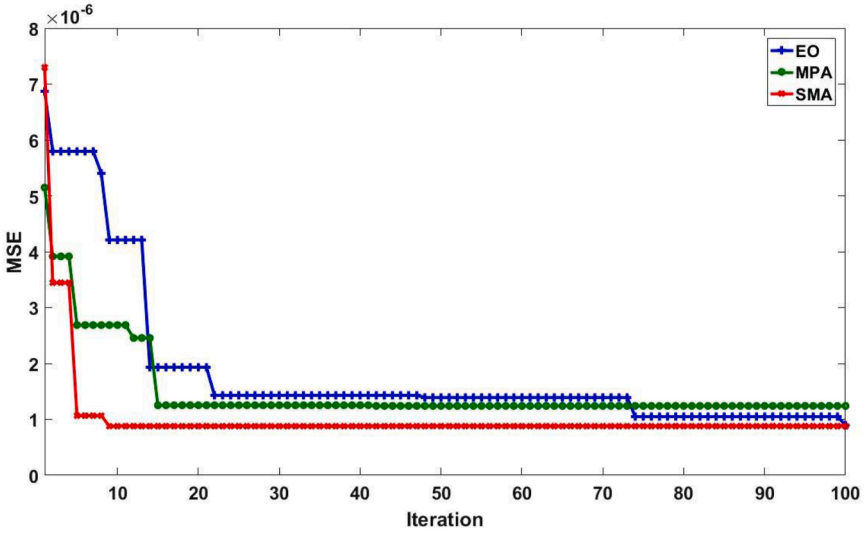

c) 4HL network

Fig. 14. Performance evolution for Case 1.

Table 4
Comparison of the best results for Case 1.

	N_i (number of neurons)	F_i (transfer function)	MSE	R
1HL network	[4]	[tansig]	8.1188e-07	0.99904
2HL network	[4 2]	[logsig tansig]	2.6935e-07	0.99968
3HL network	[4 2 2]	[logsig logsig logsig]	3.4525e-07	0.99959
4HL network	[4 1 1 1]	[tansig logsig tansig tansig]	8.7855e-07	0.99895

concentration (position) plays as a search agent. The search agents arbitrarily upgrade their concentration concerning best-so-far solutions, namely equilibrium candidates, to achieve the equilibrium state (optimal result) finally. More details on EO can be found in Faramarzi et al. [51].

4.2. Marine predator algorithm (MPA)

MPA is a swarm-based algorithm proposed by Faramarzi et al. [46], inspired by marine predators' behavior, including monitor lizards, sharks, sunfish, and etc. [52]. Marine predator algorithm generally includes three phases. In phase 1, the prey moves faster than the predator; the predator adopts the Brownian movement as its predation strategy. In phase 2, the prey and predator move at approximately the similar speed.

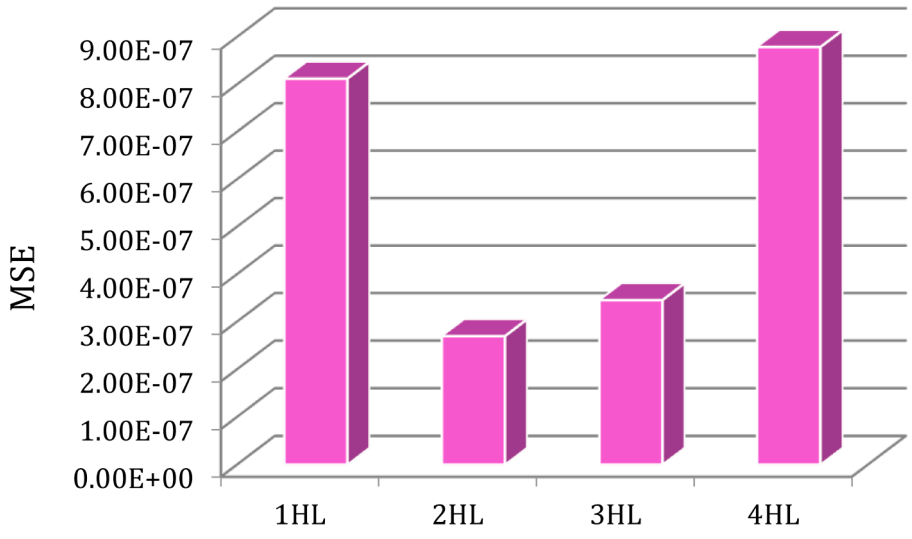

a) MSE

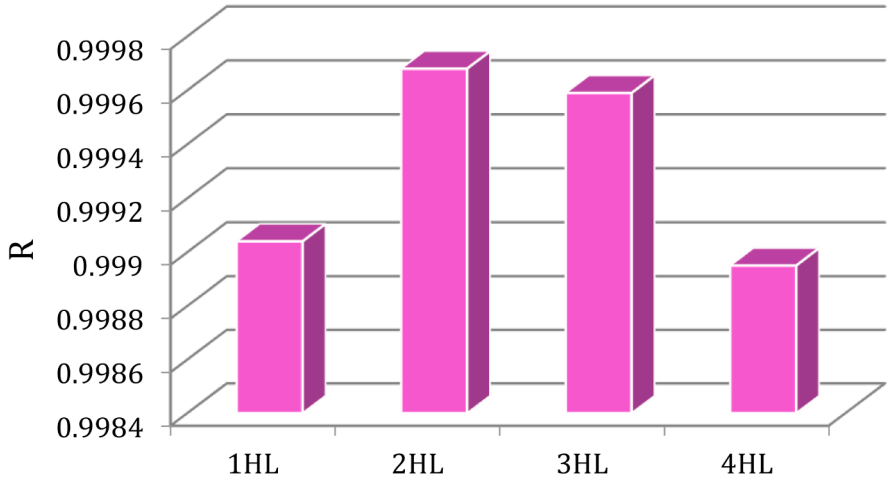

b) R

Fig. 15. Comparison of the best results for Case 1.

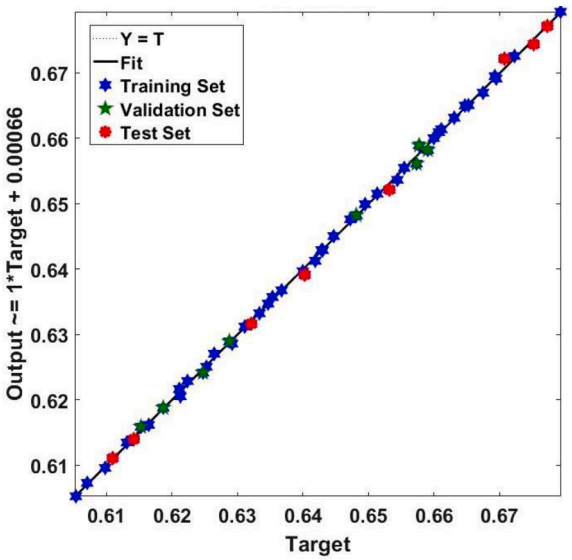

a) Regression diagram (R=0.99968)

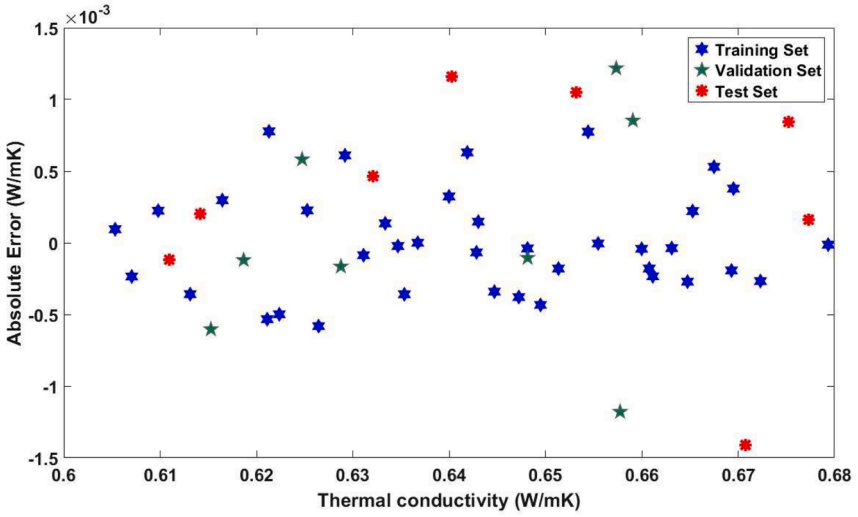

b) Absolute Error

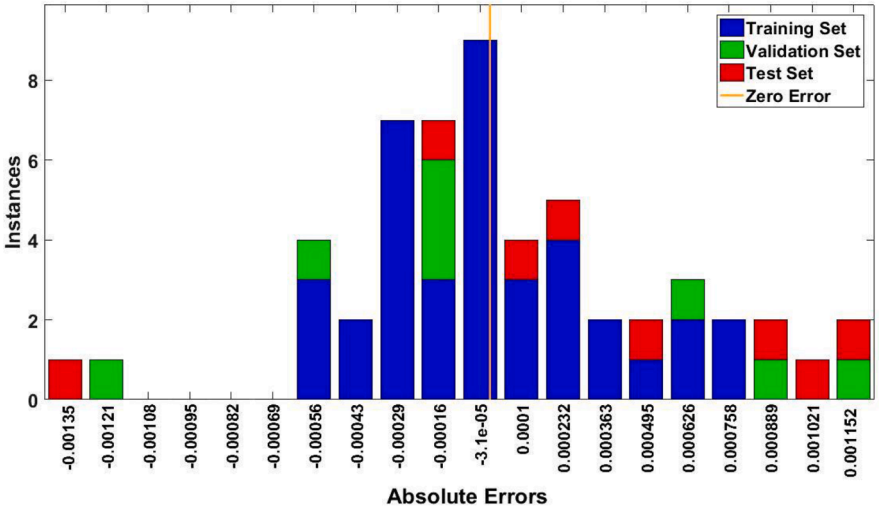

c) Error histogram

Fig. 16. Error analysis for Case 1 with the best network.

Table 5
Optimum values of the design parameters in Case 2.

Network	Algorithms	N_i (number of neurons)	F_i (transfer function)	MSE	R
2HL	EO	[9 30]	[tansig logsig]	6.3315e-04	0.99935
	MPA	[4 6]	[logsig tansig]	8.6517e-04	0.99917
	SMA	[7 1]	[tansig tansig]	8.0538e-04	0.99918
3HL	EO	[9 2 1]	[logsig elliotsig elliotsig]	7.9801e-04	0.99919
	MPA	[7 2 1]	[tansig logsig tansig]	9.3501e-04	0.99904
	SMA	[5 1 1]	[tansig tansig tansig]	1.0937e-03	0.99889
4HL	EO	[7 30 17 6]	[logsig tansig logsig tansig]	1.0461e-03	0.99917
	MPA	[6 7 3 3]	[logsig logsig logsig logsig]	8.5247e-04	0.99913
	SMA	[6 1 1 2]	[tansig elliotsig tansig tansig]	1.2113e-03	0.99883

The adopted strategy of the predator is to implement Brownian and Lévy movements at the same time. Half of the predators of the population carry out the Lévy movement, and the other half implement the Brownian movement. In phase 3, the predator moves faster than the prey; the strategy adopted by the predator is the Lévy movement. More details on MPA and its optimization scenarios, along with the Brownian and Lévy movements can be found in Faramarzi et al. [46].

4.3. Slime mould algorithm (SMA)

SMA is a swarm-based algorithm, and the slime mould is classified as a fungus with a venous network to find food. The slime mould can approach food according to the odor in the air, then the contraction of the venous tissue wraps food contacted by vein. Without having any brain or neurons, slime moulds are exceptionally brilliant, capable of solving complex computational problems with high efficiency [53]. The slime mould can memorize, make motion decisions and contribute to changes [54]. This organism can optimize the form of its network as time passes by getting more information [54]. They take three main steps; (1) approach food based on the odor in the air, (2) wrap food by the venous tissue, and (3) propagate wave by the biological oscillator, so that they tend to be in a better position of food concentration. Heretofore, the SMA solved many real-world optimization problems in industry and science better than many competitive algorithms such as PSO. For example, the SMA integrated with other population-based solvers is used for COVID-19 chest X-ray images [55]. More details on SMA can be found in Li et al. [50].

5. Result and discussion

5.1. Results for the networks with one hidden layer (1HL)

We use the results with 1HL network to compare them with those in two, three, and four hidden layers networks. Fig. 4 depicts the typical structure of the 1HL network where the optimization problem has two design variables, $X = [N_1, F_1]^T$. By considering different N_1 and F_1 values in 1∼30 and 1∼3, respectively, the problem has 90 different combinations. From the results, one can select the optimal design variables with minimum MSE without any optimization. W_i and b_i are weight and bias, respectively. The transfer function in neural networks takes an input multiplied by a weight 'W_i'. Bias (b_i) allows for shifting of the transfer function by adding a constant (i.e., the given bias) to the input. Table 2 shows the best results (i.e., the minimum MSE) for five different thermophysical properties using the 1HL network, where R is the regression value for all data.

Figs. 5–9 show the regression diagrams for the best MLP network with 1HL, based on the specifications in Table 2, for all five thermophysical parameters. These diagrams show that an MLP network with 1 HL can predict the desired outputs with $R > 0.97371$. The best result is for Case 3 ($R = 0.99945$), while the worst is for Case 4 ($R = 0.97371$)

5.2. Optimizing the networks with two, three, and four hidden layers

This section considers and optimizes the MLP neural network with two hidden layers (2HL), three hidden layers (3HL), and four hidden layers (4HL) using the aforementioned optimization algorithms. Figs. 10–12 show the typical structure of the 2HL, 3HL, and 4HL networks. The population sizes and the maximum iterations for all cases are chosen as 10 and 100 for the optimization process.

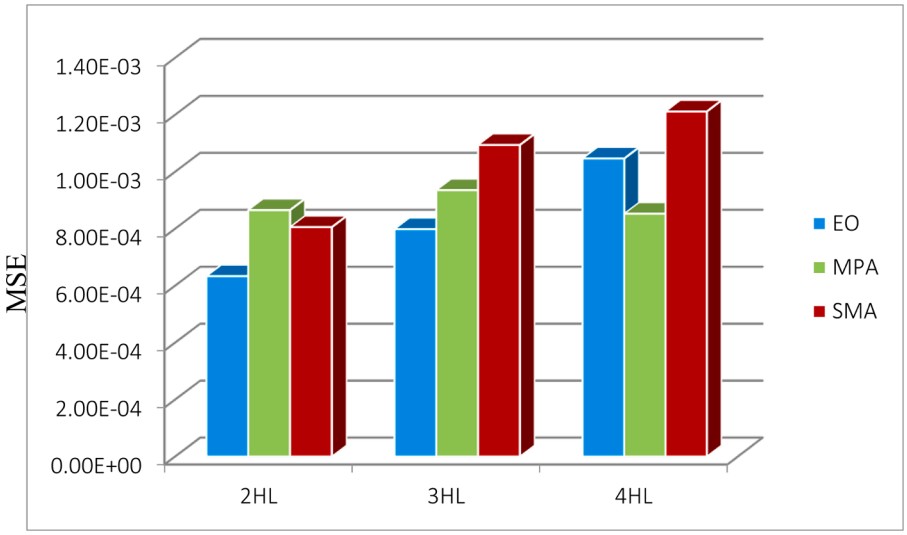

Fig. 17. Comparison between MSE errors for Case 2.

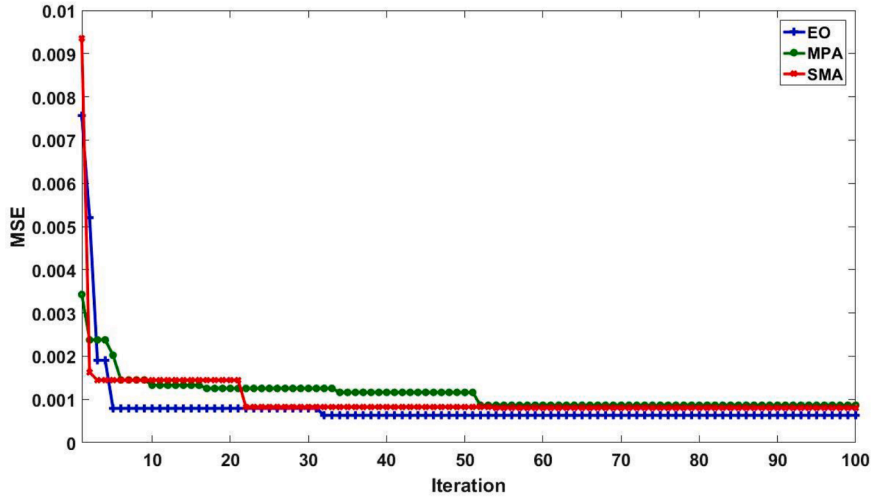

a) 2HL network

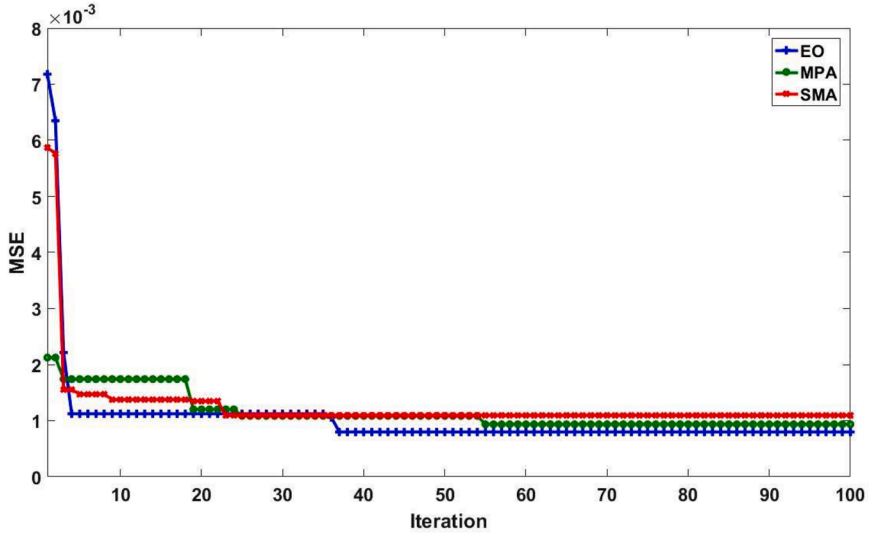

b) 3HL network

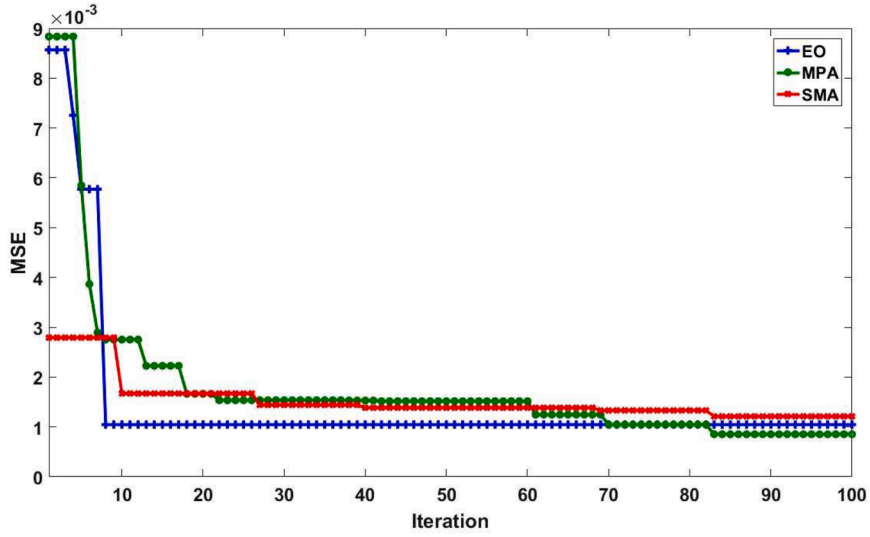

c) 4HL network

Fig. 18. Performance evolution for Case 2.

Table 6
Comparison of the best results for Case 2.

	N_i (number of neurons)	F_i (transfer function)	MSE	*R*
1HL network	[26]	[logsig]	0.001	0.99893
2HL network	[9 30]	[tansig logsig]	6.3315e-04	0.99935
3HL network	[9 2 1]	[logsig elliotsig elliotsig]	7.9801e-04	0.99919
4HL network	[6 7 3 3]	[logsig logsig logsig logsig]	8.5247e-04	0.99913

5.2.1. Case 1: thermal conductivity

The optimization results of thermal conductivity of Al_2O_3/water nanofluid using the MLP network with 2HL, 3HL, and 4HL, associated with three different algorithms including EO, MPA, and SMA, are presented in Table 3. The optimal networks, their MSE values, and the regression value are also shown. Fig. 13 compares MSE values of all applied algorithms with different hidden layer networks. This figure shows that the EO and MPA algorithms in the 2HL and 3HL networks perform better (lower MSE) than the 4HL network. Fig. 14 shows the progression of changes and reduction of MSE along with iterations for all three optimization algorithms. It must be noticed that the initial population in these methods is randomly created, which makes the starting

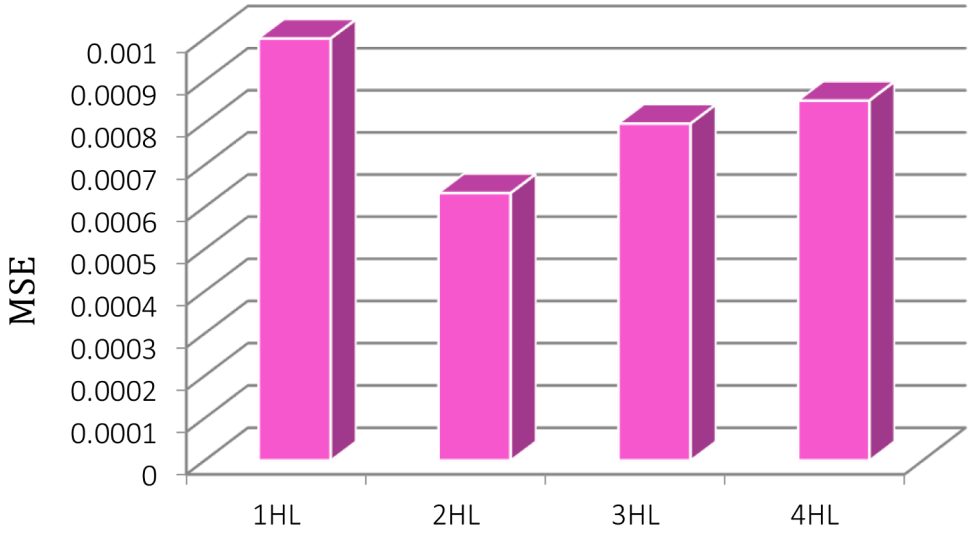

a) MSE

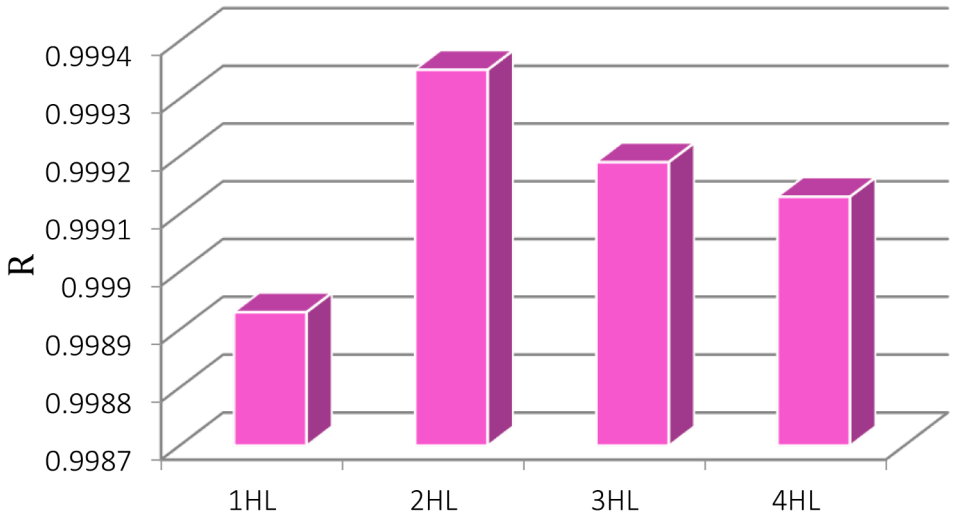

b) *R*

Fig. 19. Comparison of the best results for Case 2.

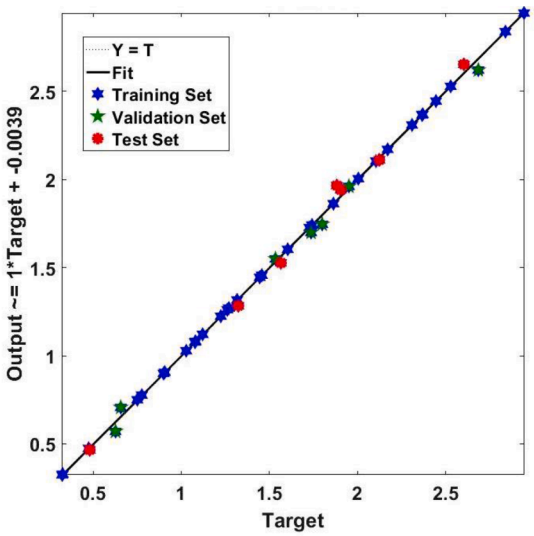

a) Regression diagram (R=0.99935)

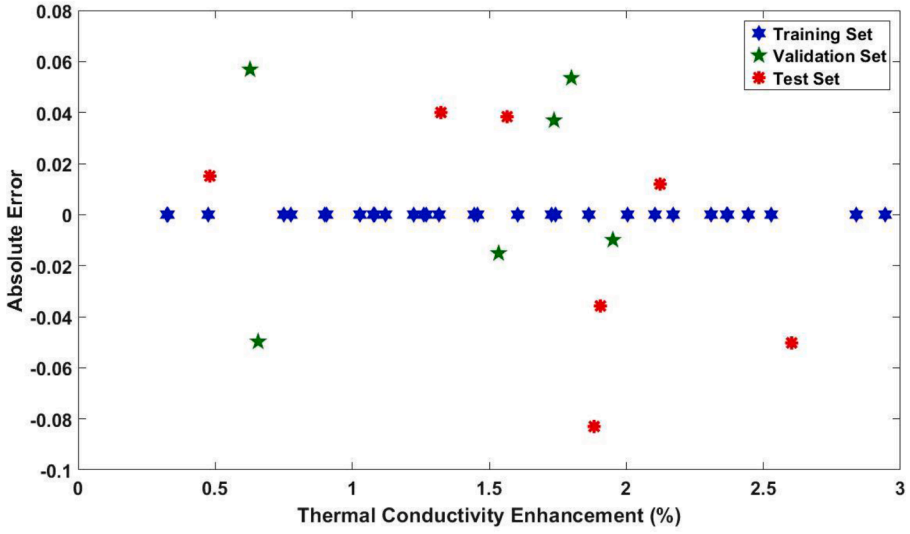

b) Absolute Error

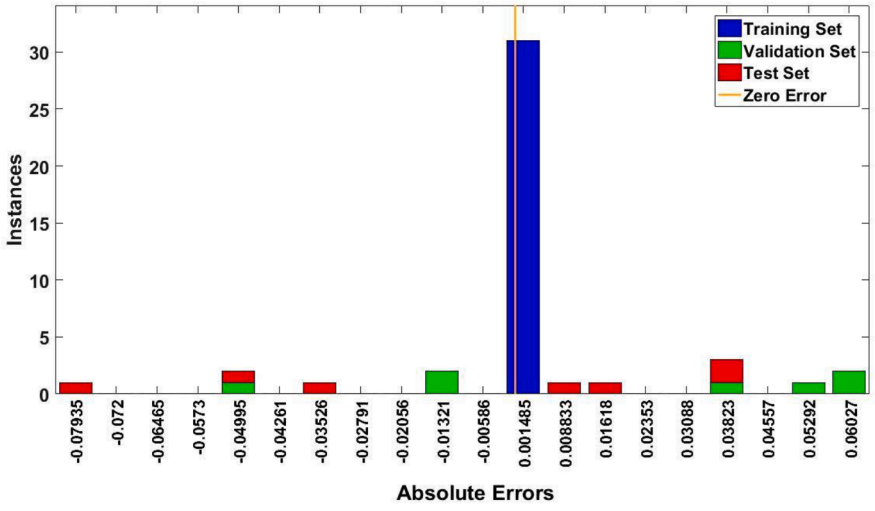

c) Error histogram

Fig. 20. Error analysis for Case 2 with the best network.

Table 7
Optimum values of the design parameters for Case 3.

Network	Algorithms	N_i (number of neurons)	F_i (transfer function)	MSE	*R*
2HL	EO	[7 3]	[logsig logsig]	5.2145e-06	0.99988
	MPA	[9 3]	[tansig logsig]	7.6667e-06	0.99984
	SMA	[6 6]	[logsig logsig]	1.0079e-05	0.99977
3HL	EO	[6 16 1]	[tansig logsig elliotsig]	4.6373e-06	0.9999
	MPA	[2 19 13]	[tansig logsig tansig]	5.7627e-06	0.99987
	SMA	[18 18 18]	[logsig logsig logsig]	1.3893e-05	0.99971
4HL	EO	[4 29 1 1]	[tansig elliotsig tansig elliotsig]	5.9626e-06	0.99986
	MPA	[4 1 1 4]	[tansig logsig elliotsig logsig]	6.3280e-06	0.99986
	SMA	[7 7 7 7]	[tansig tansig tansig tansig]	2.2263e-05	0.99955

points of the different algorithms different. The following could be observed from these results.

- In the 2HL and 3HL MLP networks, the EO and MPA algorithms perform better than the SMA algorithm.
- The SMA and EO algorithms provide better results than the MPA algorithm in the 4HL network optimization.
- The EO algorithm with the 2HL network consisting of the number of neurons N_i = [42] and the transfer functions F_i = [logsigtansig]has the lowest MSE value.
- In comparison among the transfer functions, the tansig transfer function is seen more than the other two in the optimal networks.
- Generally, the results of the EO algorithm have been better than the other two for the thermal conductivity output.
- As the number of hidden layers increases from 2 to 4, the MSE also increases.

Table 4 shows the comparison of the best results based on the number of hidden layers. This table is obtained by checking all possible scenarios for 1HL network and then performing the optimization with 2HL, 3HL, and 4HL. Fig. 15 compares MSE and *R* values of the best results in different scenarios. These results show that the network with 2HL has the best performance and creates the least error. Therefore, by increasing the number of hidden layers from 2 to 4, the MSE increase, and the *R* values decrease.

According to these results, the best network obtained for this problem is the network with 2HL; the number of neurons N_i = [42] and transfer functions F_i = [logsigtansig] obtained from the EO algorithm. Fig. 16 shows the results of error analysis in this optimal network, and Fig. 16a shows the regression diagram for the training, validation, and test datasets. The value of R = 0.99968 indicates that the obtained optimal network simulates the desired problem with the least error. Fig. 16b shows the absolute error of the modeling for the thermal conductivity output. The *x*-axis is the absolute error of the modeling, which is the difference between the target and predicted values in the neural network, and the *y*-axis is thermal conductivity.

Fig. 16b shows that the maximum error is less than 1.5×10^{-3}. Fig. 16c shows the error histogram representing the errors between target and predicted values in the neural network. This histogram indicates how predicted values are close to the target values and how the errors from the neural network are distributed. The sign of the error shows the direction of the bias. The positive error means the outputs are smaller than the targets, and the negative error means that the targets are larger than the outputs. Generally, the error distribution diagram follows the normal distribution for a precise model. Based on Fig. 16c, the error frequency accumulates mostly in the zero-axis error range, which makes a symmetric graph and shows that the methods have an excellent performance in estimating the thermal conductivity behavior in the subcooled flow boiling. Notice that the "zero error" line separates negative and positive values.

5.2.2. Case 2: thermal conductivity enhancement

Table 5 shows the results of the MLP network optimization with 2HL, 3HL, and 4HL, MSE values, and the regression values (*R*) for thermal conductivity enhancement. Fig. 17 shows the comparison between the MSE values of different algorithms with different hidden layer networks. Fig. 18 shows the progression of changes and reduction of MSE along with iterations for all three optimization algorithms. The following could be observed from these results.

- The EO algorithm performs better with the 2HL and 3HL networks than the 4HL network.
- The MPA and EO algorithms perform better results than SMA in the optimization of the 4HL network.

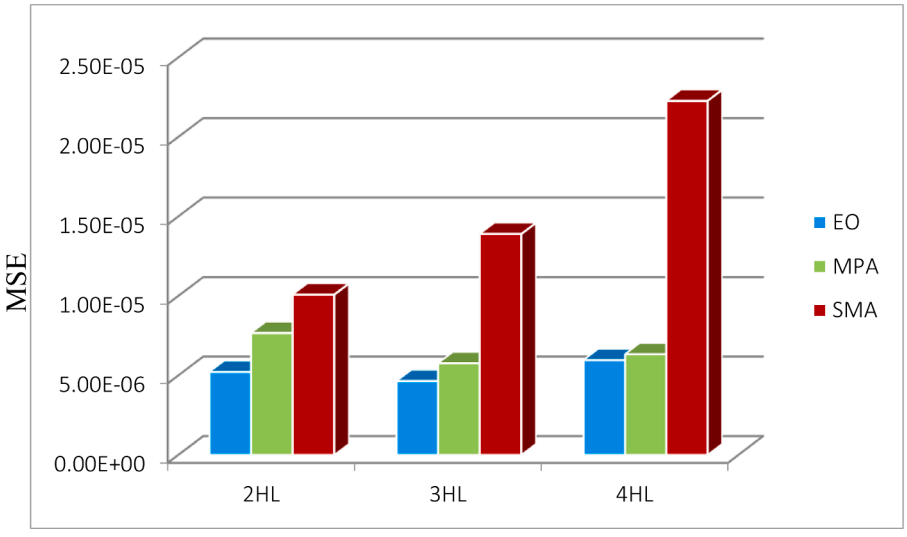

Fig. 21. Comparison between MSE values for Case 3.

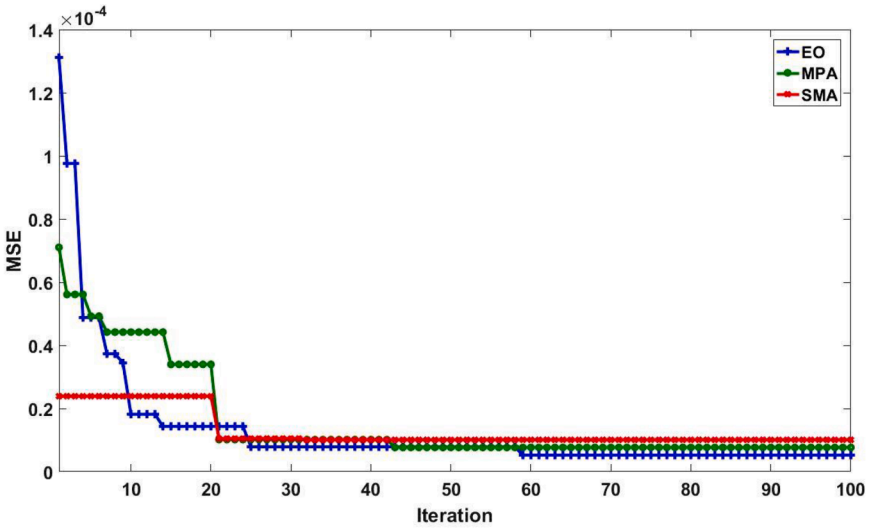

a) 2HL network

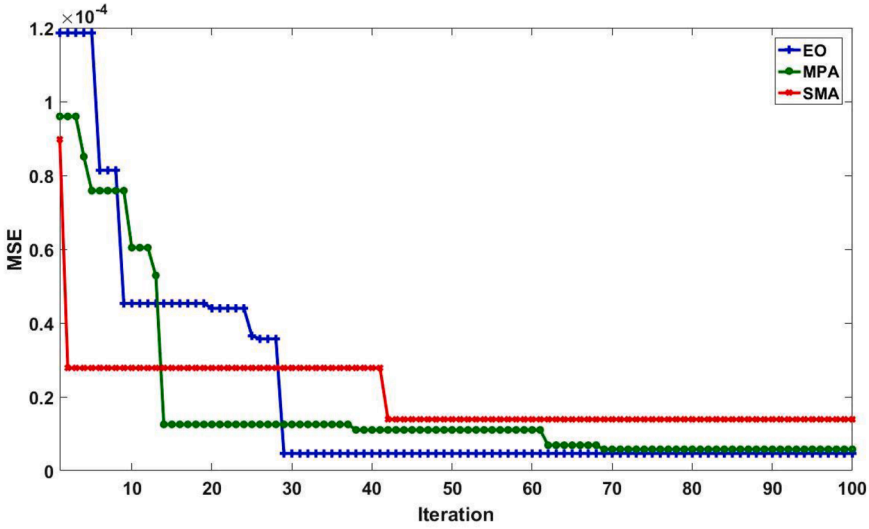

b) 3HL network

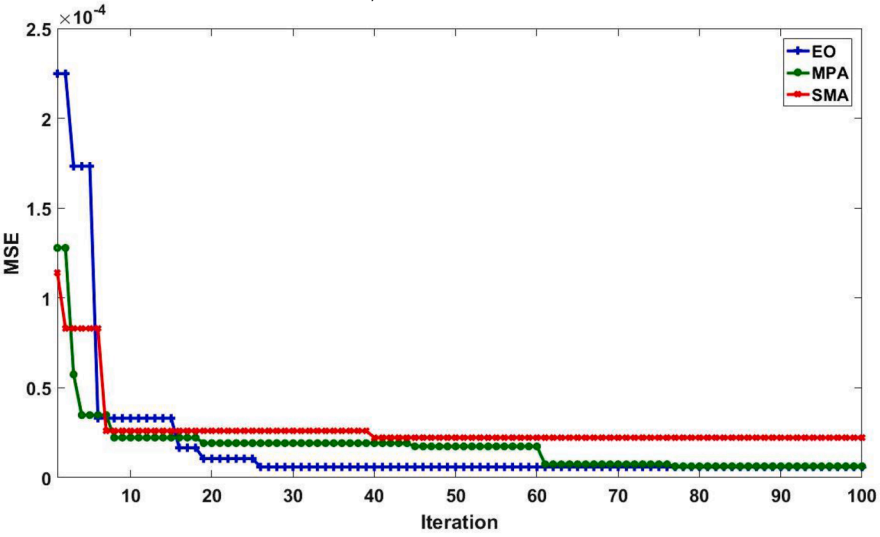

c) 4HL network

Fig. 22. Performance evolution for Case 3.

Table 8
Comparison of the best results for Case 3.

	N_i (number of neurons)	F_i (transfer function)	MSE	*R*
1HL network	[5]	[elliotsig]	2.4214e-05	0.99945
2HL network	[7 3]	[logsig logsig]	5.2145e-06	0.99988
3HL network	[6 16 1]	[tansig logsig elliotsig]	4.6373e-06	0.9999
4HL network	[4 29 1 1]	[tansig elliotsig tansig elliotsig]	5.9626e-06	0.99986

- The EO algorithm with the 2HL network consisting of the number of neurons $N_i = [930]$ and the transfer functions $F_i =$ [tansiglogsig] has the lowest MSE value.
- In comparison among the transfer functions, *tansig* and *logsig* are more commonly seen in optimal networks than *elliotsig*.
- The EO algorithm performs better than the other two algorithms.
- As the number of hidden layers increases from 2 to 4, the network error also increases.

Table 6 shows the comparison between the best results based on the number of hidden layers. The least MSE value can be obtained using the 2HL network, which is 6.3315×10^{-4}. Fig. 19 compares the best results based on the MSE and *R* values. According to these results, the network with 2HL has the best performance and creates the least error among all the networks. Therefore, by increasing the number of hidden layers from 2 to 4, the MSE values increase, and the *R* values decrease.

Based on these results, the best network obtained for this problem was the network with 2 hidden layers optimized by the EO algorithm. The number of neurons and the transfer functions is$N_i = [930]$and $F_i =$ [tansiglogsig], respectively. Fig. 20 shows the results of error analysis in this optimal network. Fig. 20a shows the regression diagram for the training, validation, and test datasets close to 1 (R=0.99935), showing that the network can accurately model the desired output. The amount of error for the thermal conductivity enhancement and the error

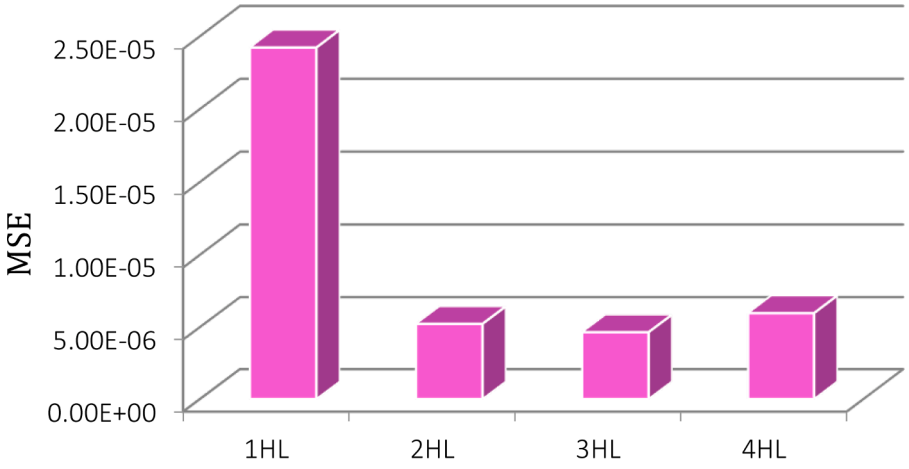

a) MSE

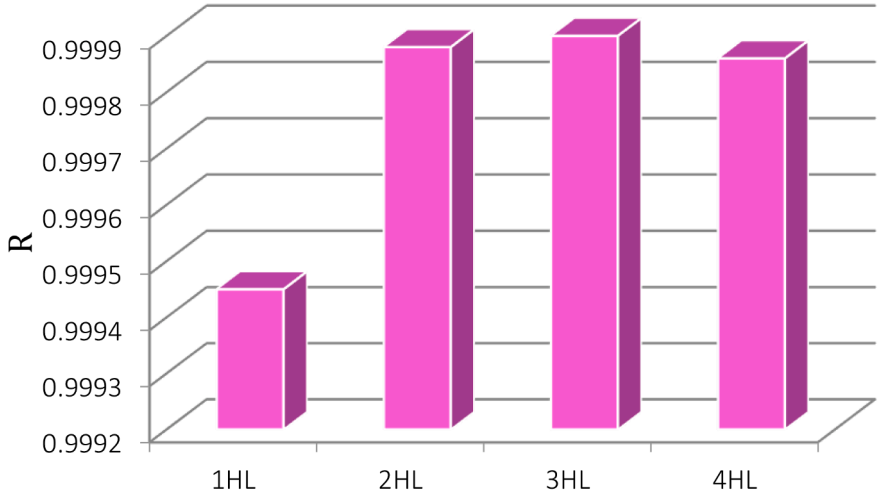

b) *R*

Fig. 23. Comparison of the best results for Case 3.

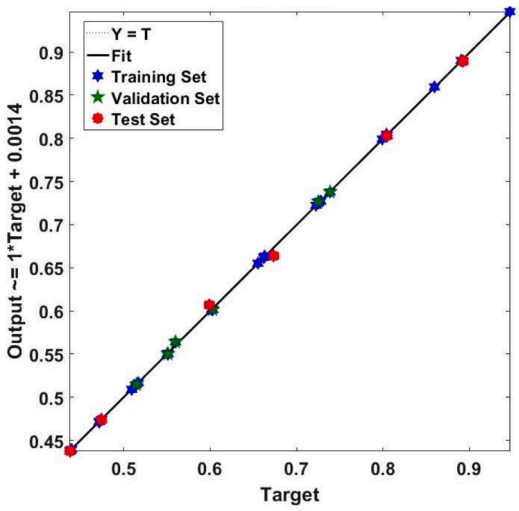

a) Regression diagram (R=0.9999)

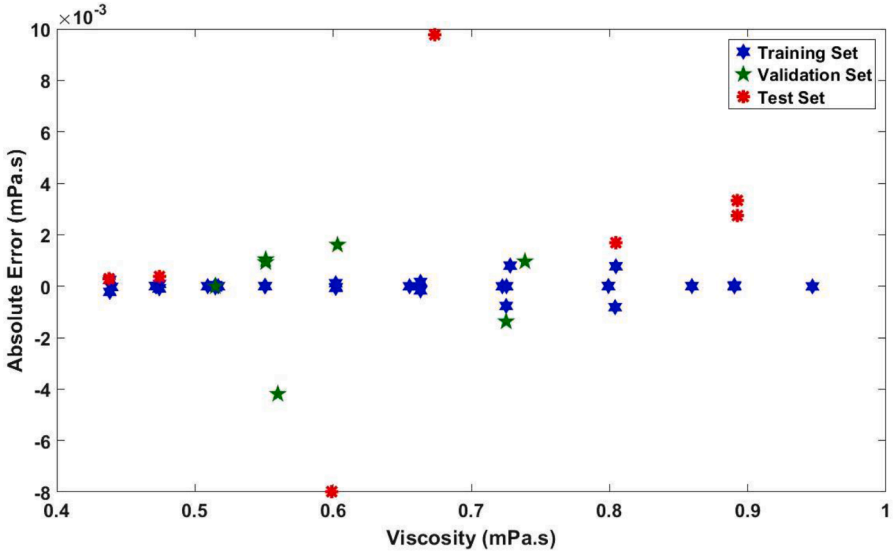

b) Absolute Error

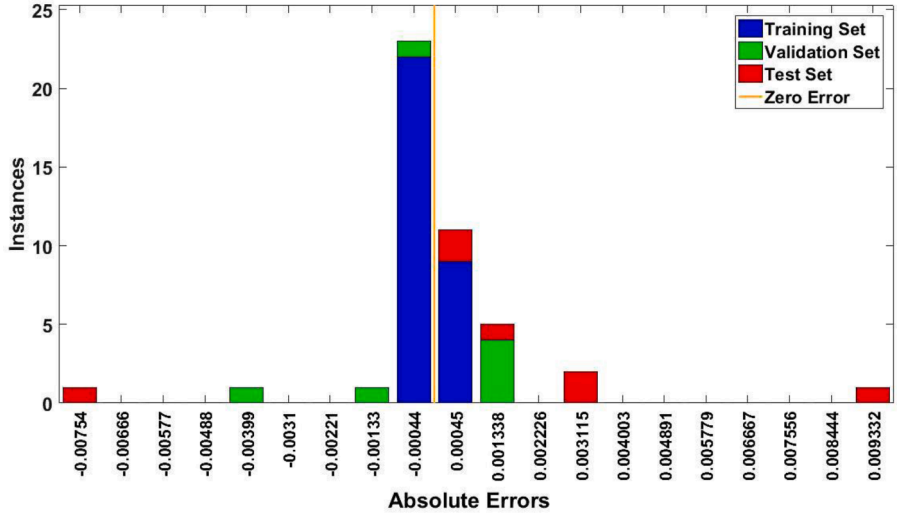

c) Error histogram

Fig. 24. Error analysis for Case 3 with the best network.

Table 9
Optimum values of the design parameters for Case 4.

Network	Algorithms	N_i (number of neurons)	F_i (transfer function)	MSE	*R*
2HL	EO	[18 25]	[tansig tansig]	0.1423	0.99302
	MPA	[30 11]	[logsig logsig]	0.0685	0.99666
	SMA	[26 30]	[logsig logsig]	0.1812	0.99140
3HL	EO	[23 20 14]	[elliotsig logsig logsig]	0.0667	0.99677
	MPA	[30 12 2]	[logsig tansig logsig]	0.0598	0.99707
	SMA	[29 28 18]	[logsig tansig elliotsig]	0.1269	0.99405
4HL	EO	[26 27 14 13]	[logsig logsig tansig tansig]	0.1208	0.99421
	MPA	[30 14 11 14]	[logsig tansig tansig logsig]	0.1280	0.99378
	SMA	[23 17 22 18]	[logsig tansig tansig tansig]	0.1456	0.99382

histogram are shown in Fig. 20-b and 20-c, respectively. The value of $R = 0.99935$ and the displayed errors indicate that the obtained optimal network could simulate the desired problem with the least error.

5.2.3. Case 3: viscosity

The optimization results of viscosity are presented in Table 7. The comparison between MSE values of different algorithms with different hidden layers networks is also shown in Fig. 21. Fig. 22 shows the progression of changes and reduction of MSE along with iterations for all three optimization algorithms. The following could be observed from these results.

- In optimization for all three types of networks (2HL, 3HL, and 4HL), the EO algorithm followed by the MPA algorithm has obtained better results than SMA.
- The SMA algorithm has the worst performance in all three types of networks.
- The EO algorithm with the 3HL network consisting of the number of neurons N_i = [6161]and the transfer functions F_i = [tansiglogsigelliotsig] has the lowest MSE value.
- In comparison among transfer functions, tansig and logsig functions are seen more than elliotsig in optimal networks.
- A network with 3HL leads to the lowest MSE for this problem.

Table 8 shows the comparison between the best results based on the number of hidden layers. This table shows that the best network for this problem is the 3HL network, whose MSE value is 4.6373×10^{-6}. Fig. 23 also compares MSE and *R* values of the best results in different scenarios. These results show that the number of hidden layers for this problem should be more than 1 to achieve a lower MSE. Also, the difference between optimal networks with 2HL, 3HL, and 4HL is small, but a network with 3HL is the most appropriate network and leads to the least error.

As mentioned, the best network obtained for this problem is the network with 3HL optimized by the EO algorithm, in which the number of neurons and transfer functions are N_i = [6161] and F_i = [tansiglogsigelliotsig], respectively. Fig. 24 shows the results of error analysis in this optimal network, and Fig. 24-a shows the regression diagram for all the output data. Also, the amount of error and the error histogram in training, test, and validation datasets are shown in Fig. 24-b and 24-c, respectively. The value of R= 0.9999 and the displayed errors indicate that the obtained optimal network was able to model the desired problem with the least error.

5.2.4. Case 4: viscosity enhancement

The optimization results of viscosity enhancement, including optimal networks, their MSE values, and the regression value (*R*), are presented in Table 9. Fig. 25 shows the comparison between the MSE values of all applied optimization algorithms for viscosity enhancement with different hidden layers networks. Fig. 26 shows the progression of changes and reduction of MSE along with iterations for all three optimization algorithms. The following results can be summarized based on the findings:

- The MPA algorithm followed by the EO algorithm performs better in optimizing 2HL and 3HL networks than the SMA algorithm.
- The EO and the MPA algorithms provide better results in the 4HL network optimization than the SMA.
- Overall, the MPA algorithm achieves the best result (lower MSE value) for modeling the viscosity enhancement data.
- The SMA algorithm has the weakest performance in all three types of networks.

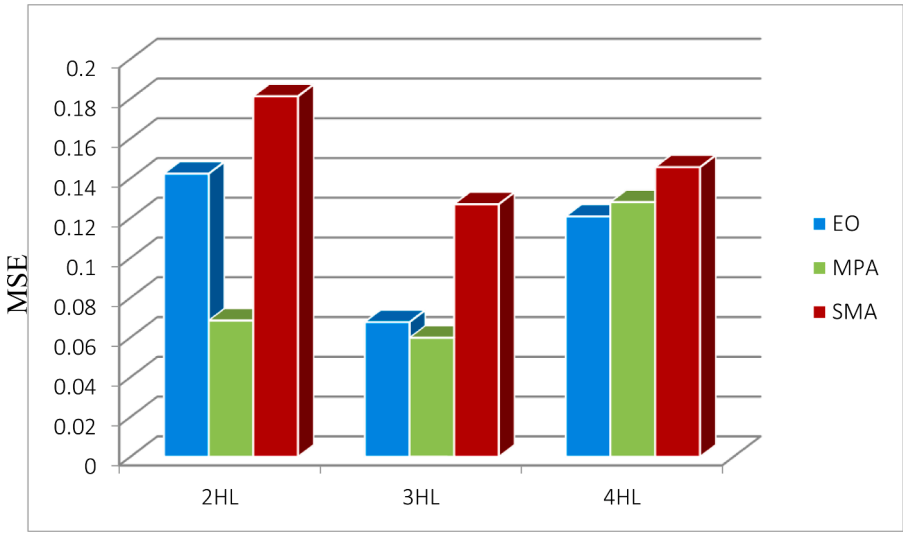

Fig. 25. Comparison between MSE values for Case 4.

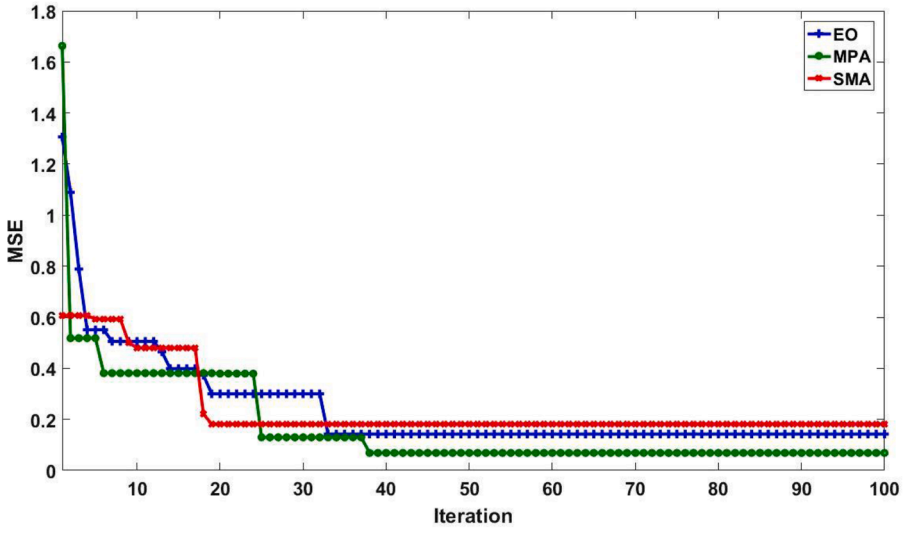

a) 2HL network

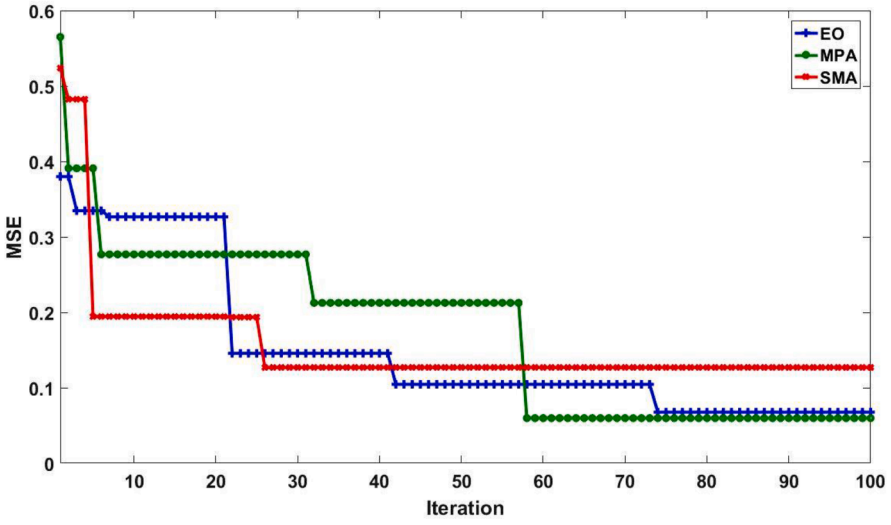

b) 3HL network

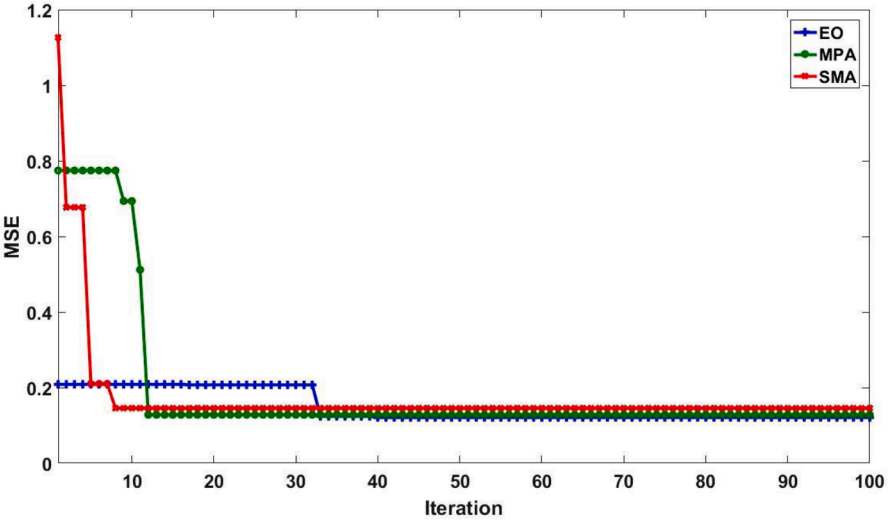

c) 4HL network

Fig. 26. Performance evolution for Case 4.

Table 10
Comparison of the best results for Case 4.

	$\mathbf{N_i}$ (number of neurons)	$\mathbf{F_i}$ (transfer function)	MSE	R
1HL network	[16]	[tansig]	0.5423	0.97371
2HL network	[30 11]	[logsig logsig]	0.0685	0.99666
3HL network	[30 12 2]	[logsig tansig logsig]	0.0598	0.99707
4HL network	[26 27 14 13]	[logsig logsig tansig tansig]	0.1208	0.99421

- The MPA algorithm with the 3HL network consisting of the number of neurons N_i = [30122] and transfer functions F_i = [logsigtansiglogsig] has the lowest MSE value.
- In comparison among transfer functions, the *elliotsig* function is less seen than the other two in optimal networks.
- The network with 3HL has better performance (lower MSE values) for this problem.

Table 10 shows the comparison between the best results based on the number of hidden layers. Fig. 27 also compares the best results based on MSE and R values. It can be concluded that the number of hidden layers must be more than 1 to have a model with a low MSE value. Also, it should be noticed that although the difference between optimal networks with two and three hidden layers is small, a network with three hidden layers is the most appropriate network, which leads to the least error.

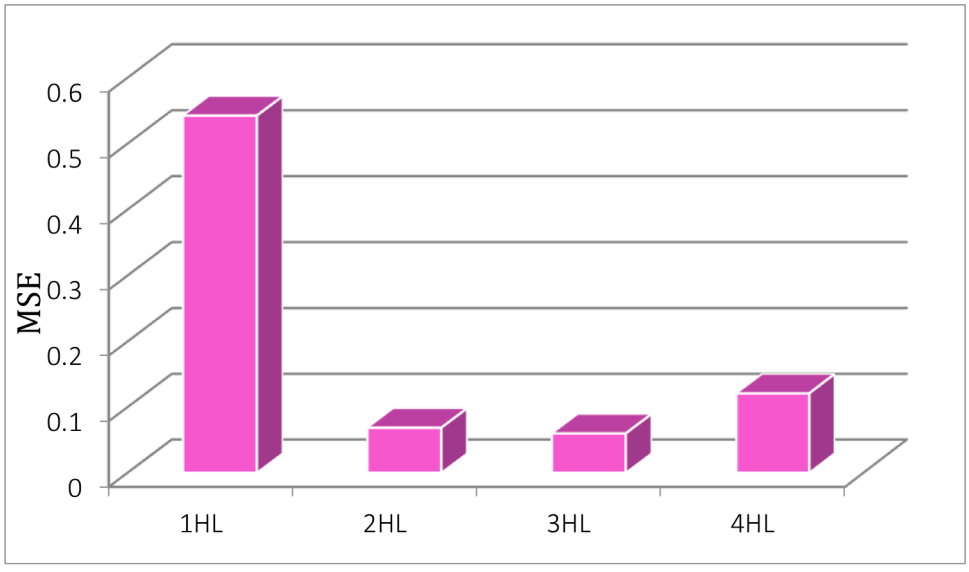

a) MSE

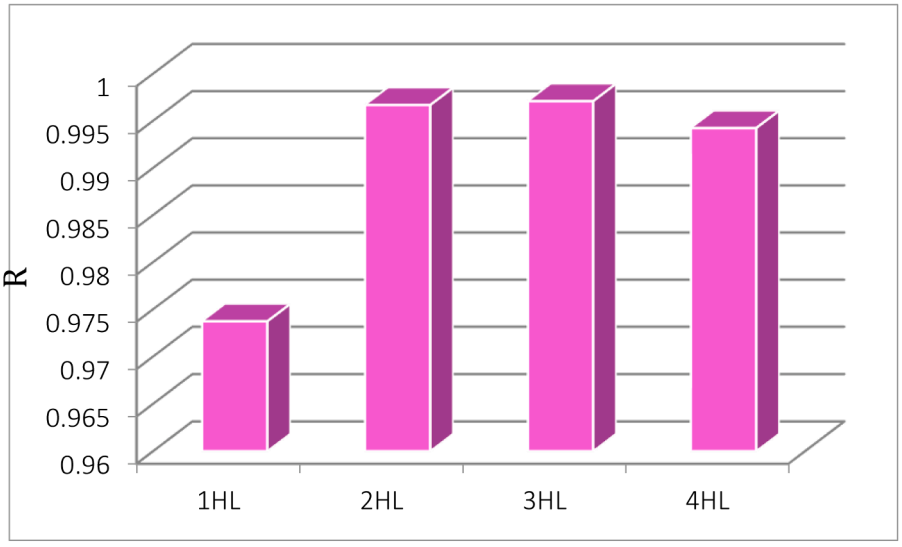

b) R

Fig. 27. Comparison of the best results for Case 4.

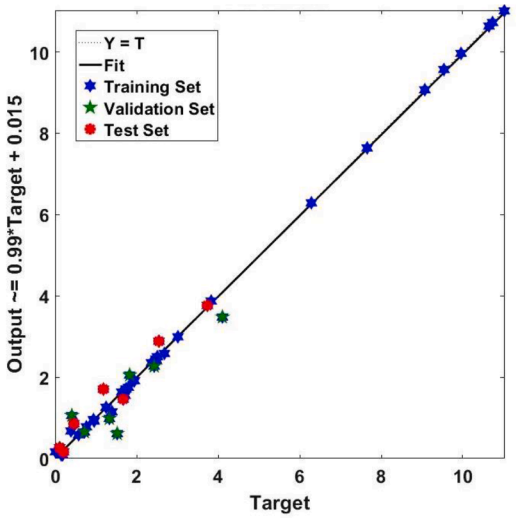

a) Regression diagram (R=0.99707)

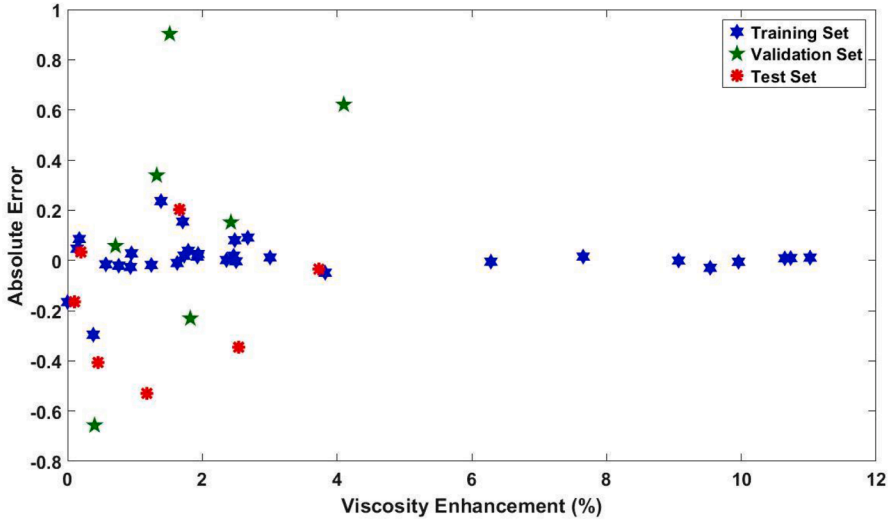

b) Absolute Error

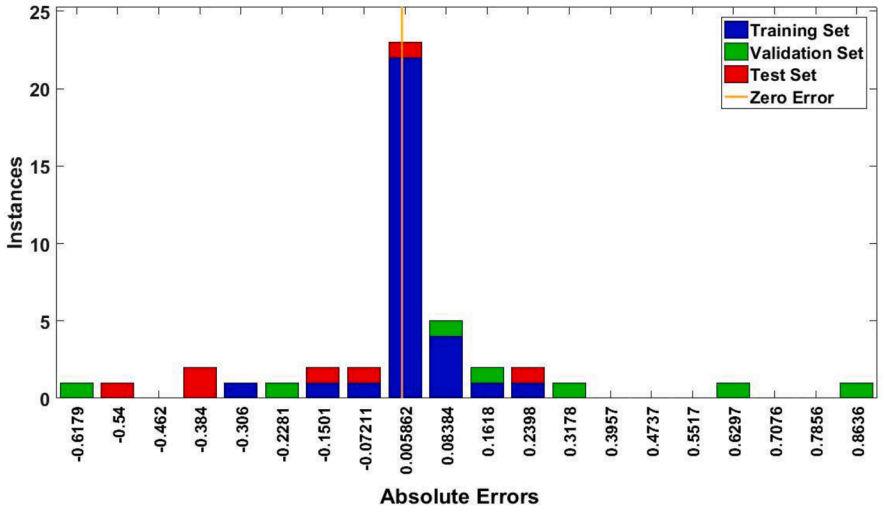

c) Error histogram

Fig. 28. Error analysis for Case 4 with the best network.

Table 11
Optimum values of the design parameters for Case 5.

Network	Algorithms	N_i (number of neurons)	F_i (transfer function)	MSE	*R*
2HL	EO	[11 3]	[tansig elliotsig]	14.1977	0.99805
	MPA	[4 11]	[tansig tansig]	10.2501	0.99858
	SMA	[8 3]	[tansig elliotsig]	13.1251	0.99819
3HL	EO	[3 22 17]	[logsig logsig logsig]	17.9319	0.99757
	MPA	[4 9 4]	[tansig elliotsig elliotsig]	14.7558	0.99802
	SMA	[5 21 27]	[tansig logsig logsig]	16.9460	0.99765
4HL	EO	[4 13 20 4]	[logsig logsig tansig tansig]	27.3904	0.99626
	MPA	[5 9 12 11]	[tansig logsig tansig tansig]	30.6425	0.99578
	SMA	[4 28 3 2]	[logsig logsig elliotsig elliotsig]	20.3954	0.99719

According to Table 7 and Fig. 27, the best network for modeling the viscosity enhancement is the network with 3HL derived from the MPA algorithm. In this network, the number of neurons and the transfer functions are N_i = [30122] and F_i = [logsigtansiglogsig], respectively. Fig. 28 examines the error in this optimal network. Fig. 28-a shows the regression diagram for all the output data. Table 2 shows that the viscosity enhancement output is the most difficult of the five problems discussed since it has a lower *R*-value than other parameters. The error rates at different outputs and the error histograms are shown in Figs. 28-b and 28-c, respectively, indicating that the obtained optimal network has acceptable accuracy and can model the desired output.

5.2.5. Case 5: heat transfer coefficient

The optimization results of the heat transfer coefficient are presented in Table 11. Also, the comparison between MSE values of all three optimization algorithms for the heat transfer coefficient with different hidden layers networks is represented in Fig. 29. Fig. 30 shows the progression of changes and reduction of MSE along with iterations for all three optimization algorithms. The following could be observed from these results.

- The MPA algorithm followed by the SMA algorithm performed better in optimizing 2HL and 3HL networks compared with the EO algorithm.
- The SMA and EO algorithms perform better than the MPA (lower MSE and higher *R*) in 4HL network optimization.
- The SMA algorithm performs better for modeling the heat transfer coefficient than the previous 4 problems.
- Compared to the previous 4 problems, the EO algorithm performs worse in this problem.
- The MPA algorithm with the 2HL network consisting of the number of neurons N_i = [411] and the transfer functions F_i = [tansigtansig] has the lowest MSE value.
- Based on Fig. 29, the network with 2HL has the best performance for this problem.

Table 12 shows the comparisons between the best results based on the number of hidden layers. Fig. 31 also compares the best results based on MSE and *R* values. According to these results, the network with 2HL has the best performance, which leads to the least error. Therefore, by increasing the number of hidden layers from 2 to 4, the MSE values increase, and the *R* values decrease.

Based on Table 12 and Fig. 31, the best network for this problem is the 2HL network with the number of neurons N_i = [411]and transfer functions F_i = [tansigtansig] derived from the MPA algorithm. Fig. 32 examines the error in this optimal network. Fig. 32-a shows the regression diagram for the training, validation, and test datasets. The value of *R*=0.99858 indicates that the obtained optimal network can model the desired problem with an acceptable error. Also, the amount of error in different datasets and the error histogram are shown in Fig. 32-b and 32-c, respectively.

6. Comparison between different cases

In this study, the actual data (and not the normalized data) of the flow boiling of Al_2O_3/water nanofluids in a horizontal tube (5 outputs in Table 1) has been used. Therefore the MSE values of the networks are very different in the 5 different problems. In other words, the MSE values are in different ranges. Hence, the *R* values of each optimization are used to compare the results from different cases—the closer the *R*-value to 1, the better the network's performance.

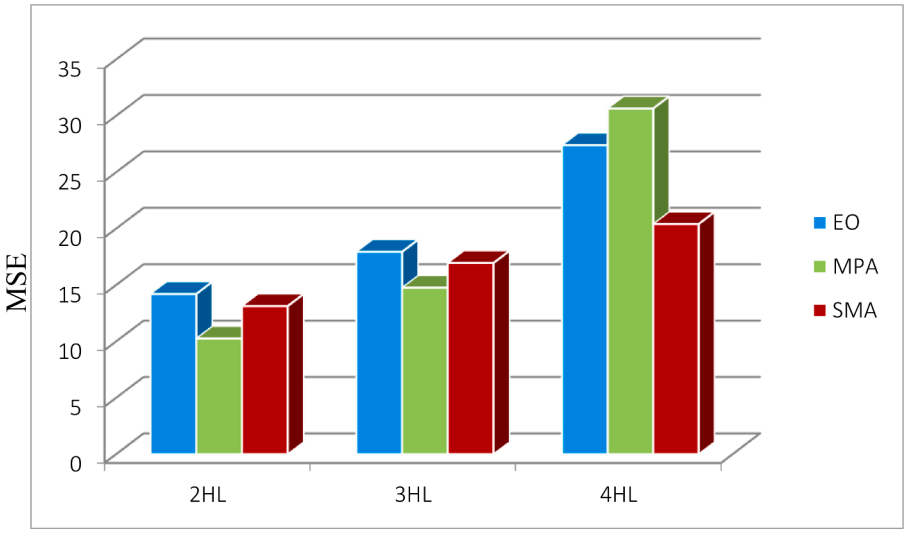

Fig. 29. Comparison between MSE errors for Case 5.

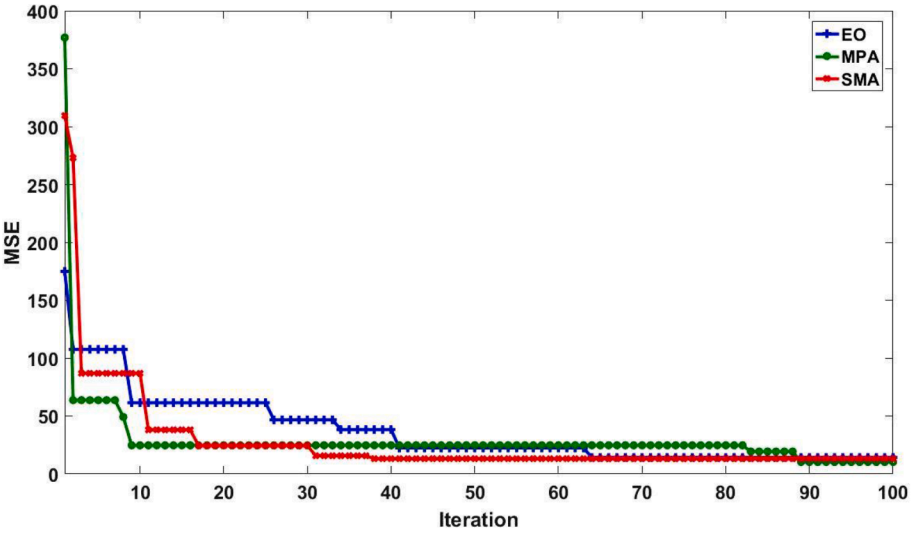

a) 2HL network

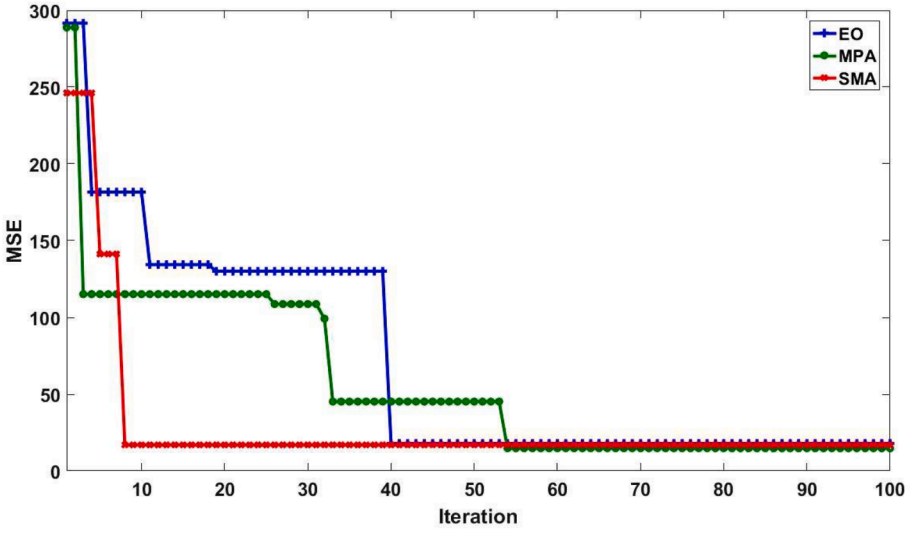

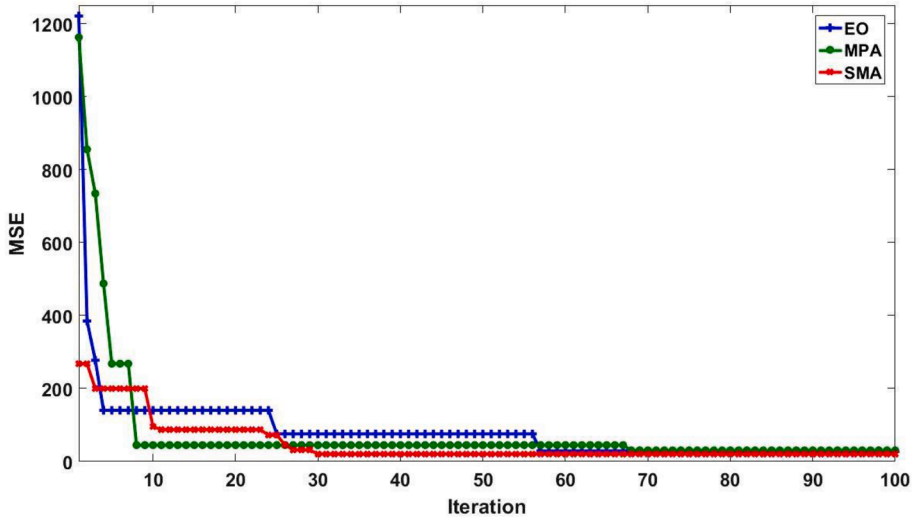

c) 4HL network

Fig. 30. Performance evolution for Case 5.

Table 12
Comparison of the best results for Case 5.

	N_i (number of neurons)	F_i (transfer function)	MSE	*R*
1HL network	[9]	[tansig]	33.7358	0.99532
2HL network	[4 11]	[tansig tansig]	10.2501	0.99858
3HL network	[4 9 4]	[tansig elliotsig elliotsig]	14.7558	0.99802
4HL network	[4 28 3 2]	[logsig logsig elliotsig elliotsig]	20.3954	0.99719

Fig. 33 summarizes the *R* values for the optimal networks of 5 outputs with the three optimization algorithms. It clearly shows that the applied MLP networks and the optimizations can model the values of the thermal conductivity, thermal conductivity enhancement, and viscosity better than the other two outputs, namely viscosity enhancement and heat transfer coefficient. In comparison between these outputs, the best performance of the model is the viscosity, while the weakest performance is related to the viscosity enhancement.

Table 13 compares the optimization results for the 5 outputs from another perspective: which type of network is the best and which algorithm has extracted the optimal network. Recall from the results of the previous sections that the EO algorithm achieves the best network for the first three outputs, thermal conductivity, thermal conductivity enhancement, and viscosity. In comparison, the MPA algorithm extracts

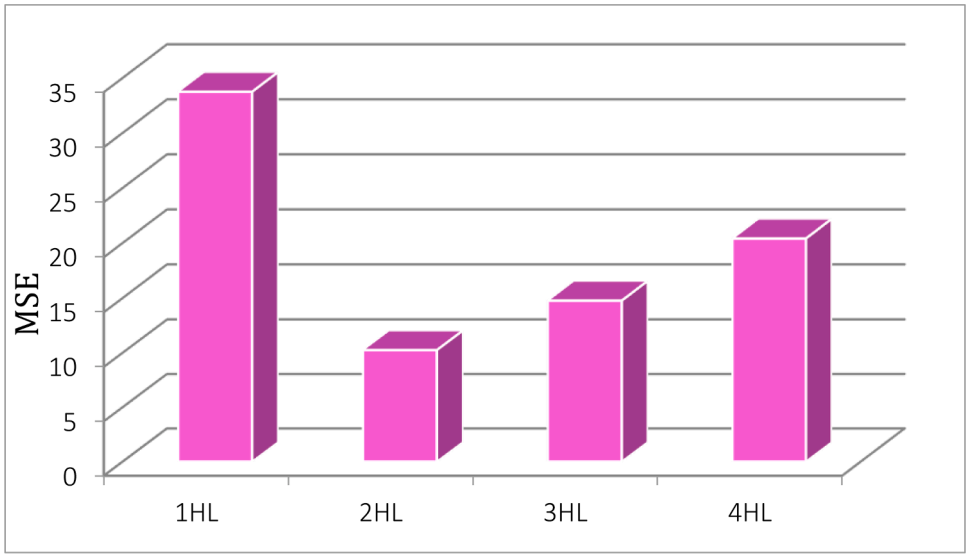

a) MSE

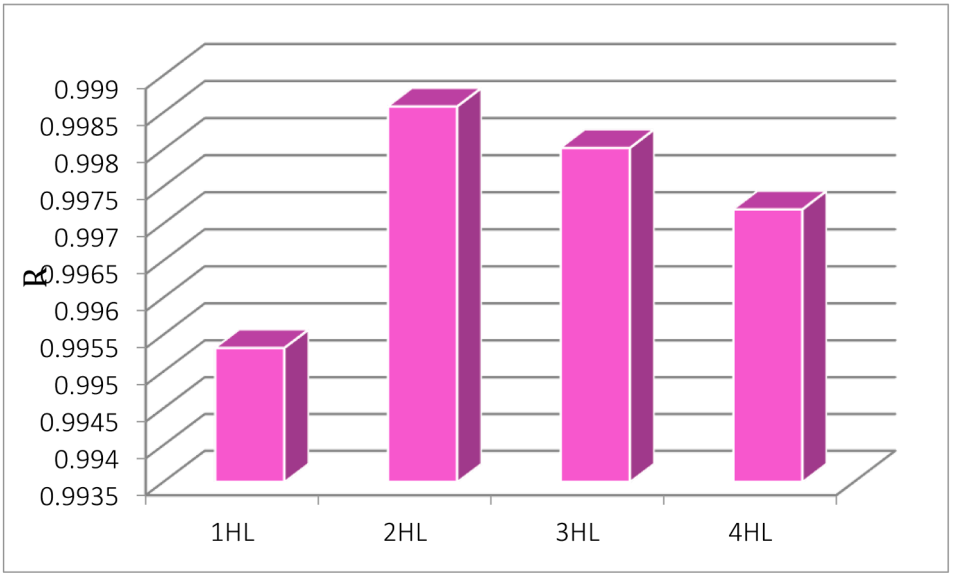

b) R

Fig. 31. Comparison of the best results for Case 5.

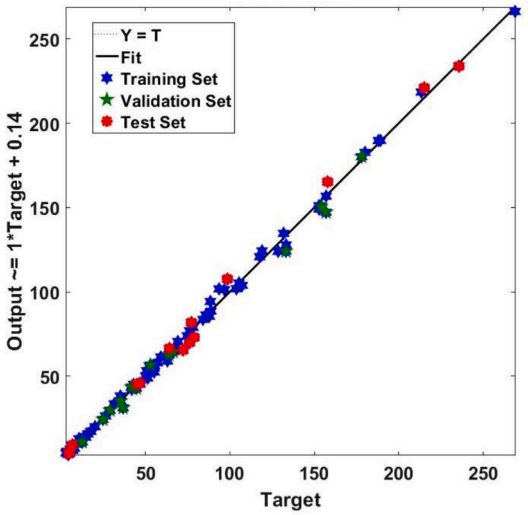

a) Regression diagram (R=0.99858)

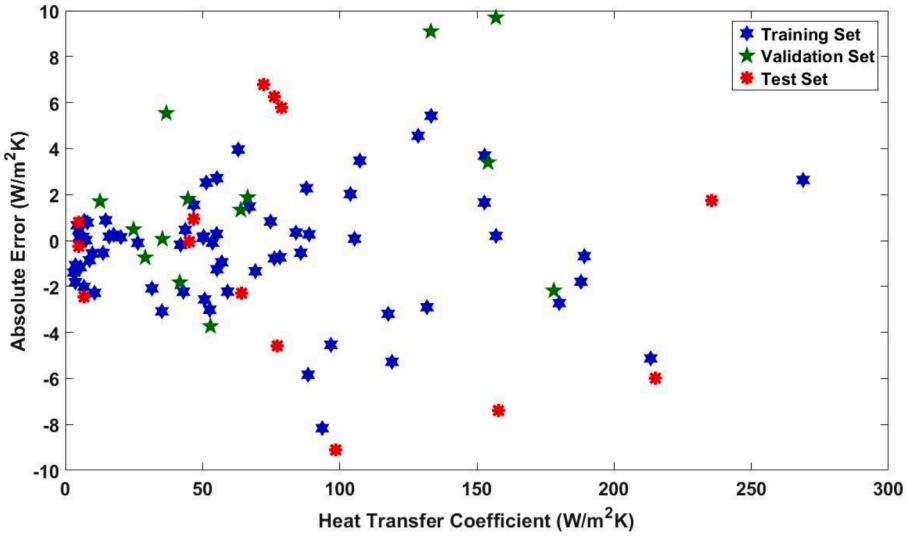

b) Absolute Error

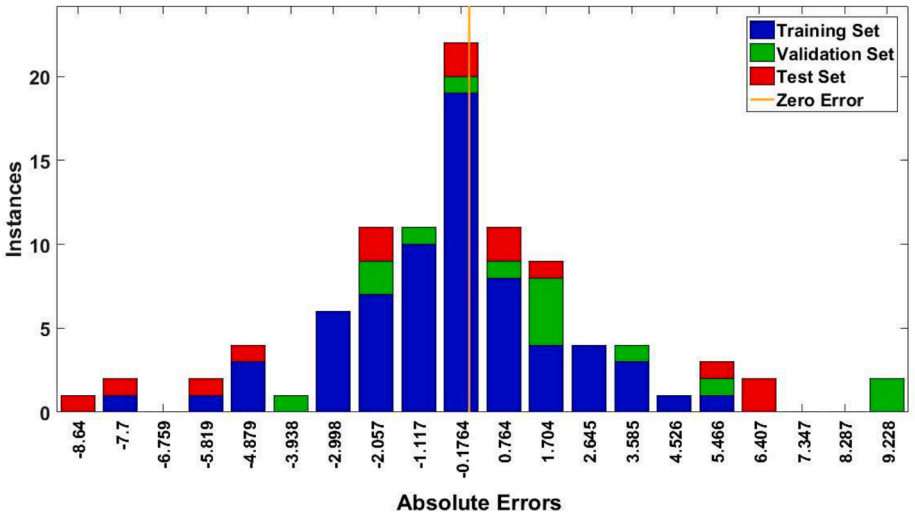

c) Error histogram

Fig. 32. Error analysis for Case 5 with the best network.

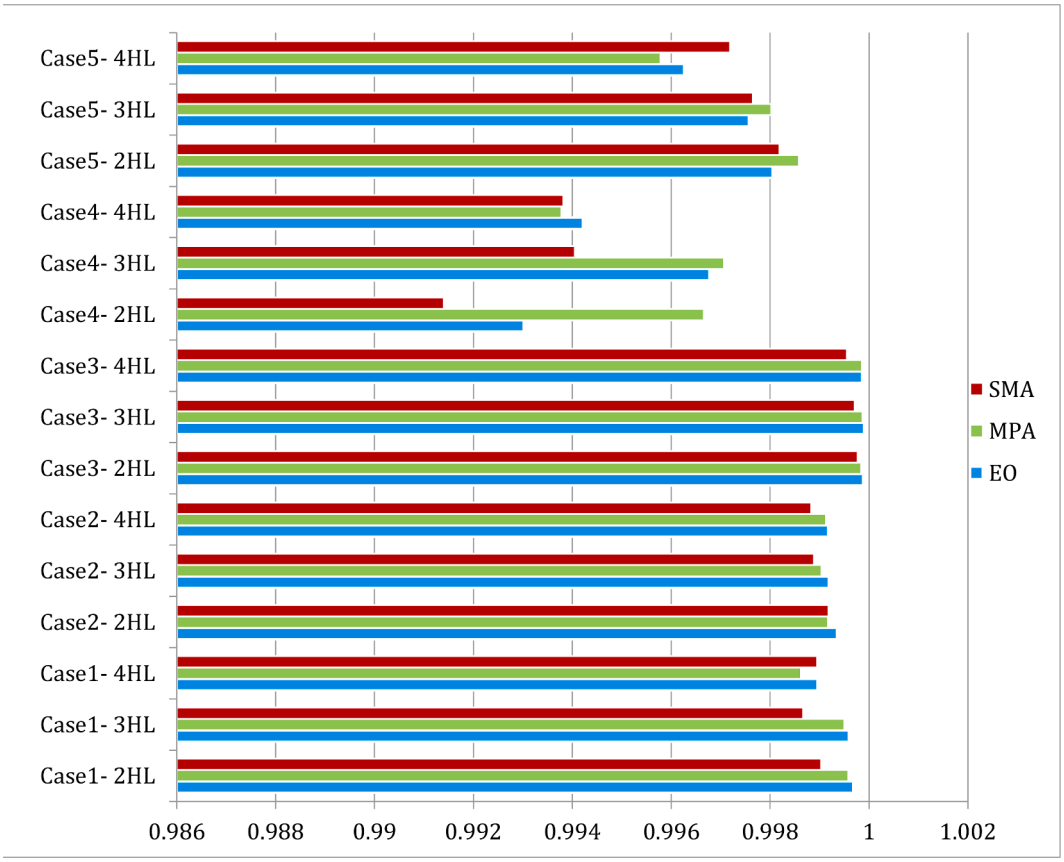

Fig. 33. Optimal network's *R-value* for different cases.

Table 13
Best network and algorithm for each output.

Best Algorithm	Best Network	Output of the system
EO	2HL	Thermal Conductivity
EO	2HL	Thermal Conductivity Enhancement
EO	3HL	Viscosity
MPA	3HL	Viscosity Enhancement
MPA	2HL	Heat Transfer Coefficient

the optimal network for the other two outputs, viscosity enhancement and heat transfer coefficient. Also, the network with 2HL is the best for the thermal conductivity, thermal conductivity enhancement, and heat transfer coefficient. In contrast, the network with 3HL performs the best performance for the viscosity and viscosity enhancement.

Fig. 34 shows another comparison between the three optimization algorithms concerning the mean value of *R* between 15 different implementations, corresponding to Fig. 33. It can be seen that the MPA and EO algorithms are significantly better than the SMA algorithm for modeling the flow boiling of Al_2O_3/water nanofluid in a horizontal tube.

7. Conclusion

In this paper, a multilayer perceptron (MLP) ANN with a back-propagation (BP) training algorithm is applied for modeling thermo-physical properties and subcooled flow boiling performance of Al_2O_3/water nanofluid in a horizontal tube. The modeling data focuses on the influences of the nanofluid concentration, heat flux, and flow rate on different thermophysical parameters, including thermal conductivity, thermal conductivity enhancement, viscosity, viscosity enhancement, and heat transfer coefficient are investigated. Specifically, flow boiling of Al_2O_3/water nanofluid in a horizontal tube with the MLP neural network optimized by three novel swarm-based optimization algorithms, namely: Equilibrium Optimizer (EO), Marine Predators Algorithm (MPA), and Slime Mould Algorithm (SMA), is modeled. To evaluate the effectiveness of different optimization models, the MSE and *R* values that allow us to determine the best optimization network are calculated and compared. The results of MLP network optimization with three algorithms are summarized as follows:

- The applied neural network and the optimizations can model the values of the thermal conductivity, thermal conductivity enhancement, and viscosity better than the other two outputs, namely viscosity enhancement and heat transfer coefficient. In comparison between these outputs, the best performance of the model is the viscosity values, while the worst performance is related to the viscosity enhancement.
- By comparing the optimization results for the 5 outputs, the EO algorithm performs the best for the thermal conductivity, thermal conductivity enhancement, and viscosity, while the MPA algorithm extracts the optimal network for the viscosity enhancement and heat transfer coefficient.
- In optimization with 2HL and 3HL networks for the thermal conductivity, the EO and the MPA algorithms perform better than the SMA algorithm.
- The EO algorithm with 2HL is the best network for modeling the thermal conductivity and thermal conductivity enhancement.
- The EO algorithm with 3HL is the best network for modeling the viscosity.
- The MPA algorithm with 3HL is the best network to model the viscosity enhancement, while the MPA with 2HL is the best network for modeling the heat transfer coefficient.

In general, the comparison of the three optimization algorithms in

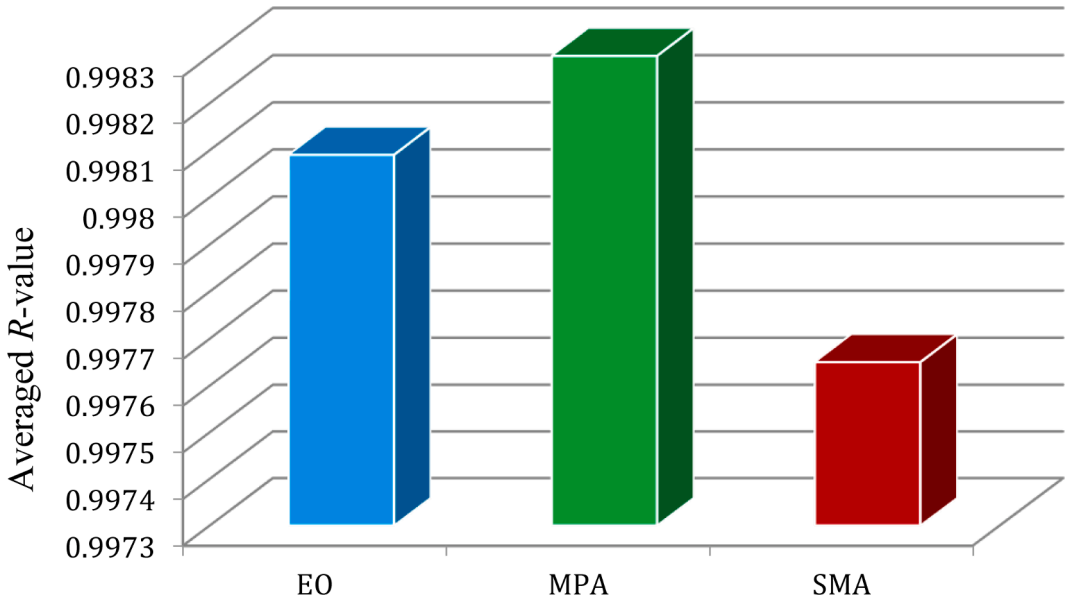

Fig. 34. Averaged R for all 15 cases.

terms of the mean value of R between 15 different implementations shows that the MPA and EO algorithms are significantly better than the SMA algorithm for modeling the flow boiling of Al_2O_3/water nanofluid in a horizontal tube.

Author agreement statement

We declare that this manuscript is original, has not been published before and is not currently being considered for publication elsewhere.

We confirm that the manuscript has been read and approved by all named authors and that there are no other persons who satisfied the criteria for authorship but are not listed. We further confirm that the order of authors listed in the manuscript has been approved by all of us.

We understand that the Corresponding Author is the sole contact for the Editorial process. He is responsible for communicating with the other authors about progress, submissions of revisions, and final approval of proofs.

Declaration of Competing Interest

None.

Data Availability

Data will be made available on request.

Acknowledgements

The authors acknowledge the financial support from the US National Science Foundation (#1917272).

References

[1] Gupta NK, Mishra S, Tiwari AK, Ghosh SK. A review of thermo physical properties of nanofluids. Mater Today Proc 2019;18:968–78. https://doi.org/10.1016/J.MATPR.2019.06.534.

[2] Ahmadi MH, Mohseni-Gharyehsafa B, Ghazvini M, Goodarzi M, Jilte RD, Kumar R. Comparing various machine learning approaches in modeling the dynamic viscosity of CuO/water nanofluid. J Therm Anal Calorim 2019;139:2585–99. https://doi.org/10.1007/S10973-019-08762-Z. 2019 1394.

[3] Choi SUSE. Enhancing thermal conductivity of fluids with nanoparticles. In: Proceedings of the Enhancing Thermal Conductivity of Fluids with Nanoparticles, International Mechanical Engineering Congress and Exhibition. San Francisco, CA; 1995. https://doi.org/10.1016/J.NANOEN.2013.02.007.

[4] Boudouh M, Gualous HL, De Labachelerie M. Local convective boiling heat transfer and pressure drop of nanofluid in narrow rectangular channels. Appl Therm Eng 2010;30:2619–31. https://doi.org/10.1016/J.APPLTHERMALENG.2010.06.027.

[5] Mukherjee S, Mishra PC, Chaudhuri P. Thermo-economic performance analysis of Al2O3-water nanofluids — an experimental investigation. J Mol Liq 2020;299:112200. https://doi.org/10.1016/J.MOLLIQ.2019.112200.

[6] Wang Y, Deng K, Wu J, Su G, Qiu S. The characteristics and correlation of nanofluid flow boiling critical heat flux. Int J Heat Mass Transf 2018;122:212–21. https://doi.org/10.1016/J.IJHEATMASSTRANSFER.2018.01.118.

[7] Peng H, Ding G, Jiang W, Hu H, Gao Y. Measurement and correlation of frictional pressure drop of refrigerant-based nanofluid flow boiling inside a horizontal smooth tube. Int J Refrig 2009;32:1756–64. https://doi.org/10.1016/J.IJREFRIG.2009.06.005.

[8] Peng H, Ding G, Jiang W, Hu H, Gao Y. Heat transfer characteristics of refrigerant-based nanofluid flow boiling inside a horizontal smooth tube. Int J Refrig 2009;32:1259–70. https://doi.org/10.1016/J.IJREFRIG.2009.01.025.

[9] Lee T, Lee JH, Jeong YH. Flow boiling critical heat flux characteristics of magnetic nanofluid at atmospheric pressure and low mass flux conditions. Int J Heat Mass Transf 2013;56:101–6. https://doi.org/10.1016/J.IJHEATMASSTRANSFER.2012.09.030.

[10] Abdolbaqi MK, Sidik NAC, Aziz A, Mamat R, Azmi WH, Yazid MNAWM, Najafi G. An experimental determination of thermal conductivity and viscosity of BioGlycol/water based TiO_2 nanofluids. Int Commun Heat Mass Transf 2016;77:22–32. https://doi.org/10.1016/J.ICHEATMASSTRANSFER.2016.07.007.

[11] Azmi WH, Sharma KV, Sarma PK, Mamat R, Najafi G. Heat transfer and friction factor of water based TiO2 and SiO2 nanofluids under turbulent flow in a tube. Int Commun Heat Mass Transf 2014;59:30–8. https://doi.org/10.1016/J.ICHEATMASSTRANSFER.2014.10.007.

[12] Prajapati OS, Rohatgi N. Flow boiling heat transfer enhancement by using ZnO-water Nanofluids. Sci Technol Nucl Install 2014;2014. https://doi.org/10.1155/2014/890316.

[13] Sarafraz MM, Abad ATK. Statistical and experimental investigation on flow boiling heat transfer to carbon nanotube-therminol nanofluid. Phys A Stat Mech Its Appl 2019;536:122505. https://doi.org/10.1016/J.PHYSA.2019.122505.

[14] Mahbubul IM, Khan MMA, Ibrahim NI, Ali HM, Al-Sulaiman FA, Saidur R. Carbon nanotube nanofluid in enhancing the efficiency of evacuated tube solar collector. Renew Energy 2018;121:36–44. https://doi.org/10.1016/J.RENENE.2018.01.006.

[15] Menbari A, Alemrajabi AA. Analytical modeling and experimental investigation on optical properties of new class of nanofluids (Al_2O_3–CuO binary nanofluids) for direct absorption solar thermal energy. Opt. Mater. 2016;52:116–25. https://doi.org/10.1016/J.OPTMAT.2015.12.023 (Amst).

[16] Jatinder G, Ohunakin OS, Adelekan DS, Atiba OE, Daniel AB, Singh J, Atayero AA. Performance of a domestic refrigerator using selected hydrocarbon working fluids and TiO_2–MO nanolubricant. Appl Therm Eng 2019;160:114004. https://doi.org/10.1016/J.APPLTHERMALENG.2019.114004.

[17] Ahmed MS, Elsaid AM. Effect of hybrid and single nanofluids on the performance characteristics of chilled water air conditioning system. Appl Therm Eng 2019;163:114398. https://doi.org/10.1016/J.APPLTHERMALENG.2019.114398.

[18] Qi C, Luo T, Liu M, Fan F, Yan Y. Experimental study on the flow and heat transfer characteristics of nanofluids in double-tube heat exchangers based on thermal efficiency assessment. Energy Convers Manag 2019;197:111877. https://doi.org/10.1016/J.ENCONMAN.2019.111877.

[19] Sarafraz MM, Pourmehran O, Yang B, Arjomandi M. Assessment of the thermal performance of a thermosyphon heat pipe using zirconia-acetone nanofluids. Renew Energy 2019;136:884–95. https://doi.org/10.1016/J.RENENE.2019.01.035.
[20] S.U.S. Choi, J.A. Eastman, Enhanced heat transfer using nanofluids, US6221275B1, 2001.
[21] Faulkner MKD. Practical design of a 1000 W/cm2 cooling system. In: Proceedings of the semiconductor thermal measurement and management symposium. Vancouver WA, Canada; 2003. p. 223–30. in: 19th IEEE SEMI-THERM Symp.
[22] Rana KB, Agrawal GD, Mathur J, Puli U. Measurement of void fraction in flow boiling of ZnO–water nanofluids using image processing technique. Nucl Eng Des 2014;270:217–26. https://doi.org/10.1016/J.NUCENGDES.2014.01.008.
[23] Sun B, Yang D. Flow boiling heat transfer characteristics of nano-refrigerants in a horizontal tube. Int J Refrig 2014;38:206–14. https://doi.org/10.1016/J.IJREFRIG.2013.08.020.
[24] Xu L, Xu J. Nanofluid stabilizes and enhances convective boiling heat transfer in a single microchannel. Int J Heat Mass Transf 2012;55:5673–86. https://doi.org/10.1016/J.IJHEATMASSTRANSFER.2012.05.063.
[25] G. Duursma, K. Sefiane, A. Dehaene, S. Harmand, Y. Wang, Flow and heat transfer of single-and two-phase boiling of nanofluids in microchannels, 10.1080/01457632.2014.994990. 36 (2015) 1252–1265. 10.1080/01457632.2014.994990.
[26] Wang Y, Wu J. Numerical simulation on single bubble behavior during Al_2O_3/H_2O nanofluids flow boiling using moving particle simi-implicit method. Prog Nucl Energy 2015;85:130–9. https://doi.org/10.1016/J.PNUCENE.2015.06.017.
[27] Wang Y, Wu J. Single bubble dynamic behavior in AL_2O_3/H_2O nanofluid on downward-facing heating surface. Nucl Eng Technol 2016;48:915–24. https://doi.org/10.1016/J.NET.2016.02.008.
[28] Wang Y, Deng K, Wu JM, Su G, Qiu S. A mechanism of heat transfer enhancement or deterioration of nanofluid flow boiling. Int J Heat Mass Transf 2020;158:119985. https://doi.org/10.1016/J.IJHEATMASSTRANSFER.2020.119985.
[29] Karimzadehkhouei M, Sezen M, Şendur K, Pınar Mengüç M, Koşar A. Subcooled flow boiling heat transfer of γ-Al2O3/water nanofluids in horizontal microtubes and the effect of surface characteristics and nanoparticle deposition. Appl Therm Eng 2017;127:536–46. https://doi.org/10.1016/J.APPLTHERMALENG.2017.08.041.
[30] Sarafraz MM, Hormozi F. Comparatively experimental study on the boiling thermal performance of metal oxide and multi-walled carbon nanotube nanofluids. Powder Technol 2016;287:412–30. https://doi.org/10.1016/J.POWTEC.2015.10.022.
[31] Ghasemi A, Hassani M, Goodarzi M, Afrand M, Manafi S. Appraising influence of COOH-MWCNTs on thermal conductivity of antifreeze using curve fitting and neural network. Phys A Stat Mech Its Appl 2019;514:36–45. https://doi.org/10.1016/J.PHYSA.2018.09.004.
[32] Kim SJ, McKrell T, Buongiorno J, wen Hu L. Subcooled flow boiling heat transfer of dilute alumina, zinc oxide, and diamond nanofluids at atmospheric pressure. Nucl Eng Des 2010;240:1186–94. https://doi.org/10.1016/J.NUCENGDES.2010.01.020.
[33] Afrand M, Abedini E, Teimouri H. Experimental investigation and simulation of flow boiling of nanofluids in different flow directions. Phys E Low-Dimens Syst Nanostruct 2017;87:248–53. https://doi.org/10.1016/J.PHYSE.2016.10.026.
[34] Mukherjee S, Jana S, Chandra Mishra P, Chaudhuri P, Chakrabarty S. Experimental investigation on thermo-physical properties and subcooled flow boiling performance of Al_2O_3/water nanofluids in a horizontal tube. Int J Therm Sci 2021;159:106581. https://doi.org/10.1016/J.IJTHERMALSCI.2020.106581.
[35] Ghazvini M, Maddah H, Peymanfar R, Ahmadi MH, Kumar R. Experimental evaluation and artificial neural network modeling of thermal conductivity of water based nanofluid containing magnetic copper nanoparticles. Phys A Stat Mech Its Appl 2020:124127. https://doi.org/10.1016/j.physa.2019.124127.
[36] Ertuğrul ÖF. A novel type of activation function in artificial neural networks: trained activation function. Neural Netw 2018;99:148–57. https://doi.org/10.1016/j.neunet.2018.01.007.
[37] Rajaee T, Shahabi A. Evaluation of wavelet-GEP and wavelet-ANN hybrid models for prediction of total nitrogen concentration in coastal marine waters. Arab. J. Geosci. 2016;93(9):1–15. https://doi.org/10.1007/S12517-015-2220-X. 2016.
[38] Genç B, Tunç H. Optimal training and test sets design for machine learning. Turkish J. Electr. Eng. Comput. Sci. 2019;27:1534–45. https://doi.org/10.3906/ELK-1807-212.
[39] Ahmed AAM. Prediction of dissolved oxygen in Surma River by biochemical oxygen demand and chemical oxygen demand using the artificial neural networks (ANNs). J. King Saud Univ. Eng. Sci. 2017;29:151–8. https://doi.org/10.1016/J.JKSUES.2014.05.001.
[40] Prashanth DS, Mehta RVK, Sharma N. Classification of handwritten Devanagari number – an analysis of pattern recognition tool using neural network and CNN. Procedia Comput. Sci. 2020;167:2445–57. https://doi.org/10.1016/J.PROCS.2020.03.297.
[41] Alizadeh MJ, Kavianpour MR. Development of wavelet-ANN models to predict water quality parameters in Hilo Bay, Pacific Ocean. Mar Pollut Bull 2015;98:171–8. https://doi.org/10.1016/J.MARPOLBUL.2015.06.052.
[42] Nazari M, Varedi-Koulaei SM, Nazari M. Flow characteristics prediction in a flow-focusing microchannel for a desired droplet size using an inverse model: experimental and numerical study. Microfluid Nanofluidics 2022;26:1–19. https://doi.org/10.1007/S10404-022-02529-Z/FIGURES/20.
[43] Fijani E, Barzegar R, Deo R, Tziritis E, Konstantinos S. Design and implementation of a hybrid model based on two-layer decomposition method coupled with extreme learning machines to support real-time environmental monitoring of water quality parameters. Sci Total Environ 2019;648:839–53. https://doi.org/10.1016/J.SCITOTENV.2018.08.221.
[44] Mirjalili S, Lewis A. The whale optimization algorithm. Adv Eng Softw 2016;95:51–67. https://doi.org/10.1016/j.advengsoft.2016.01.008.
[45] Reeves C. Genetic algorithms. Handbook Metaheuristics. Boston: Kluwer Academic Publishers; 2003. p. 55–82. https://doi.org/10.1007/0-306-48056-5_3.
[46] M. Pincus, Letter to the editor-a Monte Carlo method for the approximate solution of certain types of constrained optimization problems, 18 (1970) 1225–1228. 10.1287/OPRE.18.6.1225.
[47] J. Kennedy, R. Eberhart, bls gov, Particle Swarm Optimization, n.d (2022).
[48] Faramarzi A, Heidarinejad M, Stephens B, Mirjalili S. Equilibrium optimizer: a novel optimization algorithm. Knowledge-Based Syst 2020;191:105190. https://doi.org/10.1016/J.KNOSYS.2019.105190.
[49] Faramarzi A, Heidarinejad M, Mirjalili S, Gandomi AH. Marine predators algorithm: a nature-inspired metaheuristic. Expert Syst Appl 2020;152:113377. https://doi.org/10.1016/J.ESWA.2020.113377.
[50] Li S, Chen H, Wang M, Heidari AA, Mirjalili S. Slime mould algorithm: a new method for stochastic optimization. Futur Gener Comput Syst 2020;111:300–23. https://doi.org/10.1016/J.FUTURE.2020.03.055.
[51] Faramarzi A, Heidarinejad M, Stephens B, Mirjalili S. Equilibrium optimizer: a novel optimization algorithm. Knowledge-Based Syst 2020;191:105190. https://doi.org/10.1016/j.knosys.2019.105190.
[52] Humphries NE, Queiroz N, Dyer JRM, Pade NG, Musyl MK, Schaefer KM, Fuller DW, Brunnschweiler JM, Doyle TK, Houghton JDR, Hays GC, Jones CS, Noble LR, Wearmouth VJ, Southall EJ, Sims DW. Environmental context explains Lévy and Brownian movement patterns of marine predators. Nat 2010;465:1066–9. https://doi.org/10.1038/nature09116. 2010 4657301.
[53] Jabr F. How brainless slime molds redefine intelligence. Nature 2012. https://doi.org/10.1038/NATURE.2012.11811.
[54] Adamatzky A. On attraction of slime mould Physarum polycephalum to plants with sedative properties. Nat Preced 2011:1. https://doi.org/10.1038/npre.2011.5985.1. 2011–1.
[55] Abdel-Basset M, Chang V, Mohamed R. HSMA_WOA: a hybrid novel Slime mould algorithm with whale optimization algorithm for tackling the image segmentation problem of chest X-ray images. Appl Soft Comput 2020;95:106642. https://doi.org/10.1016/J.ASOC.2020.106642.